

University of Alabama
Bureau of Engineering Research

PHASED ARRAY ANTENNA MATCHING:
SIMULATION AND OPTIMIZATION OF A
PLANAR PHASED ARRAY OF
CIRCULAR WAVEGUIDE ELEMENTS

FINAL REPORT

Contract NAS8-25894

January 1972

CR-123820

by

JAMES E. DUDGEON
Project Director
Department of Electrical Engineering

Prepared for

George C. Marshall Space Flight Center
National Aeronautics and Space Administration
Huntsville, Alabama

(NASA-CR-123820) PHASED ARRAY ANTENNA
MATCHING: SIMULATION AND OPTIMIZATION OF A
PLANAR PHASED ARRAY OF CIRCULAR WAVEGUIDE
ELEMENTS J.E. Dudgeon (Alabama Univ.,
University.) Jan. 1972 80 p

N73-11139

CSCL 09A G3/07

Unclas

46457

ABSTRACT

This report contains the development and utilization of a computer simulation of a planar phased array of circular waveguide elements. The simulation allows experimental work to be done on the computer and is directed toward the investigation of mutual coupling and wide angle impedance matching in phased arrays. Special emphasis is given to circular polarization. The aforementioned computer program has as variable inputs: frequency, polarization, grid geometry, element size, dielectric waveguide fill, dielectric plugs in the waveguide for impedance matching, and dielectric sheets covering the array surface for the purpose of wide angle impedance matching. Parameter combinations were found which produced reflection peaks interior to grating lobes, while dielectric cover sheets were successfully employed to extend the usable scan range of a phased array. The most exciting results came from the application of computer-aided optimization techniques to the design of this type of array. Different combinations of parameters were allowed to vary and several optimizations were found. As a consequence of the many separate investigations made possible by this program, some fairly general conclusions regarding polarization and WAIM effects could be made, and these are summarized.

Also included in this report are a comparison of the major methods for wide angle impedance matching, a discussion of multimode elements, and a coverage of bandwidth limits set by not having true time delay phase shifters in an array.

TABLE OF CONTENTS

	Page
ABSTRACT	1
LIST OF FIGURES	111
I. INTRODUCTION	1
II. SUPPLEMENTARY PHASED ARRAY DESIGN CONSIDERATIONS	8
A. Methods for Wide Angle Impedance Matching - A Comparison	8
1. Magill and Wheeler	9
2. Edelberg and Oliner Fences	9
3. Interconnecting Circuit Method	9
4. Multimode Elements	10
5. Use of Many Closely Spaced Elements	10
6. Electronically Tunable Networks	11
B. Multimode Array Elements for Wide Angle Scans	11
C. Bandwidth Considerations in Phased Arrays	13
III. CIRCULAR WAVEGUIDE ARRAYS	18
A. Computer Simulation of an Infinite Array of Circular Waveguides	21
1. Waveguide Interior Fields	24
2. Exterior Fields	25
3. Coupling Coefficients	30
B. Dielectric Cover Sheets and Matching Plugs	33
1. Single Cover Layers	37
2. Two Cover Layers	37
C. Waveguide Vector Modes	38
D. Free Space Wave Functions (Block functions)	39
E. Conclusions	41
1. Array Performance Observation	45
2. Computer-Aided Optimization Results	47
IV. EXPERIMENTAL RESULTS	50
A. Waveguide Simulator	50
B. Dielectric Cover Sheet Over a Small Array	56
C. Cavity-Backed Spirals	58
D. Ku-Band Spiral Array	58
APPENDIX	59
REFERENCES	72

LIST OF FIGURES

Figure	Page
2-1. Multimode Waveguide Elements Realization	12
2-2. Array Feeds	14
3-1. Circular Radiator	20
3-2. Dielectric Covered Array of Circular Waveguides	22
3-3. Planar Array Grid Geometry	23
3-4. Array Covered with Two Dielectric Sheets	35
3-5. Direction Cosine Space Showing Grating Lobe Regions (60° grid angle)	43
4-1. Rectangular Guide with Component Waves	51
4-2. Geometry of Simulated Phased Array	53
4-3. Waveguide Simulator Test Setup	54
4-4. Circularly Polarized Array of Crossed Slots (f = 1.8 GHz, d = 7 cm)	57
A-1. Array with Air-Filled Guides	60
A-2. Circularly Polarized Array of Circular Waveguide Elements	61
A-3. Array with Dielectric Filled Guides	62
A-4. Array of Circular Waveguides with Dielectric Cover	63
A-5. E-Plane Scan for Array of Circular Waveguides with Dielectric Cover Sheet	64
A-6. Array of Circular Waveguides with Dielectric Cover Sheet and Dielectric Discs	65
A-7. Optimized Array with Cover Sheet and Dielectric Plugs for Matching	66
A-8. Reflection Coefficient vs. Scan Angle	67
A-9. Array with Dielectric-Filled Waveguides: optimized (Rosenbrock) radius and dielectric constant	68

LIST OF FIGURES (Continued)

Figure	Page
A-10. Frequency Scanned Array of Air-Filled Guides	69
A-11. Rosenbrock Selection of Dielectric Plugs	70
A-12. 60° Scan Plane: Rosenbrock Selection of Dielectric Plugs	71

I. INTRODUCTION

As is well known, the variations of antenna element impedance with scan angle in electronically steered phased arrays can seriously affect radiation power efficiency with the problem being especially troublesome for wide angle scans. If an array antenna element is impedance matched to its source for broadside pointing, then any variations in its impedance due to ever present mutual coupling effects as the beam is scanned will result in available power not being radiated, but reflected back toward the array generators. As a consequence, whenever there is a premium on power or where there is a need for wider efficient scan ranges, it is important that the array be optimally impedance matched for all scan positions. It was the objective of this work to investigate and expand upon methods for improving the efficiency of phased array antennas. Most of the compensation measures considered work by providing a type of feedback which continuously adjusts so as to offset element impedance and consequent efficiency changes with scan angle. At the time of this study most of the existing work was concerned with linearly polarized sources, and so prime effort was given to extending the compensation procedures to matching of circularly polarized elements. The results of this endeavor are contained in three technical reports and this final report.

Technical Report No. 1, "Antenna Arrays: Efficiency and Efficiency Improvement Through Compensation," [1] is a presentation and analysis of the major compensation techniques for wide angle impedance matching (WAIM). The procedures described are generally separated into one of two categories. The first considers methods which rely on structures which modify the array surface environment. Examples of such are baffles and dielectric cover sheets [2]. The other category contains those methods which utilize matching schemes located behind the array surface, examples of which are Hannan's interconnecting circuit method [3] and the multimode element approach [4]. The multimode element procedure uses internal irises and discontinuities to generate higher order element modes which can hopefully be adjusted to offset mutual coupling scan variations. Since this method was omitted from Technical Report No. 1, it is included in Chapter II of this report. Also in Technical Report No. 1 is a good survey of design results for linear and planar phased arrays which should be useful to anyone needing a single-source compilation of phasing, grating lobe, and grid geometry considerations in phased arrays. A thorough coverage of array efficiency is given with two levels of approach. One treats all elements as ideal and determines maximum possible array efficiency as a function of grid geometry and spacing, and the other considers mutual coupling effects and illustrates the steps involved and the problems associated with the analysis of arrays of physical elements.

Technical Report No. 2, "Microstrip Technology and its Application to Phased Array Compensation," [5] started out as a specific investigation of the practicality of Hannan's interconnecting circuit method

for wide angle impedance matching and led to the need for a fairly thorough review of microstrip fabrication and design technology. A summary of these findings occupies the first portion of that report. Materials, element realizations using "lumped" versus "distributed" methods, processing, expected frequency and cost limits, losses, and a determination of microstrip characteristic impedance which better matches experimental measurements for lines with small w/d ratios are all included in early sections. With the preceeding as a basis, calculations are made for wide angle impedance matching an array of S-band, half-wave dipoles using Hannan's method. The design is carried all the way to the point of specifying size and component construction for the interconnecting networks using MIC techniques. It was found that the required compensating networks were realizable for the S-band case using lumped MIC deposited elements. In order to obtain some of the relatively small effective inductances and capacitances required for matching, off-resonance, parallel LC tank circuits were used so that larger value, better quality inductors and capacitors could be constructed.

Based on our study the following observations are made relative to the usefulness of the interconnecting circuit method of compensation.

Disadvantages:

1. This method requires "a priori" knowledge of array impedance variations with scan angle usually necessitating array simulation or experimental measurements. The later can be rather expensive if an array is built and then it is found that it cannot be matched satisfactorily.

2. Presently this technique is not cost competitive with some of the other matching methods, especially in terms of the cost of design time. Often a few crude calculations and some simple measurements can achieve a reasonable wide angle scan improvement using the dielectric cover sheet method, whereas great care and much time must be devoted to obtain a possibly temperamental microstrip realization. The real hope for application of Hannan's procedure would be in the future for phased arrays of the modular type which have active sources behind each antenna element. If subarrays of many such elements could be batch processed, then the production cost with interconnecting circuits would be essentially the same as without them. It would still be necessary to know mutual coupling and impedance effects prior to the subarray synthesis so that correct compensating circuitry could be specified. Although it is possible to individually trim values of L and C after the elements are fabricated, it would be foolish to rely on such adjustments for arrays with hundreds of elements. Instead it is desirable to take adequate steps to make accurate predictions of needs. Note the advantage of having computer-aided simulations describing array performance.
3. Matching networks might limit the frequency response of arrays intended for wideband operation. Five percent bandwidths, however, should not show significant degradation.

Advantages:

1. Extremely good matches are theoretically possible [6], in fact much better matches could probably be obtained than with any of the other WAIM schemes.

2. With individually adjustable compensating circuits, it would be possible to make post-fabrication system alterations. Also the capability of changing network values in the neighborhood of the array edge might alleviate some potential edge-effect problems.

Finally, Technical Report No. 2 contains many of the fabrication related problems and experiences relating to other facets of the contract program. For instance, a circularly polarized, Ku-band array of planar spirals was photolithographically produced with 5 mil wide gold conductors on an alumina substrate. Broadband baluns for feeding wideband elements were investigated, built, and tested. In addition, power limits set by using microstrip techniques and materials to realize physically small, Ku-band spiral antennas were estimated.

The spiral antenna element is analyzed in Technical Report No. 3, "Simulation of Planar Spiral Antenna Elements for Phased Arrays." With reliable computer-aided simulations and designs valid for large arrays of spiral antenna elements, future array systems using spiral elements could be made more economical and realizable. The importance of this will be especially great for operation at X-band and above where elements are physically very small (for half-wavelength spacings between elements at 15 GHz the spiral diameter has to be less than 1.0 cm), and as a consequence, exacting tolerances are required in construction. To meet these standards all the elements in a high frequency array could be formed in one operation using solid-state and microstrip deposition techniques. It seems reasonable to think that an entire "integrated" system including RF electronics, antenna elements, interconnecting circuits for wide angle compensation, phase shifters, and control circuitry could be built as a single unit using this technology. In any

event, systems requiring the above processes to produce the antenna elements are not recommended for experimental optimization since the resultant arrays are haphazard, expensive, and inflexible. Thus, if a sufficiently general computer program for simulating arrays of spiral antennas was part of the public domain, all necessary experimentation and optimization could be computerized and the availability of active arrays for X-band and Ku-band might be considerably advanced.

In Technical Report No. 3 a computer-aided solution for mutual coupling and impedance effects in a spiral antenna is obtained, and groundwork is laid for an analytic solution for arrays of Archimedian spiral radiators. Solutions use Harrington's method of moments [7] and a computer matrix inversion. It was found that conductor dimensions in the spirals are more critical in determining impedance than originally anticipated. Further, it was noted that the reactive portion is not always negligible even when dimensions are nearly those to give complementary symmetry. Some reasonably good designs are obtained.

Topics not covered in other reports are covered in this final report. In Chapter II are two important phased array design considerations which relate to the problems of wide angle impedance matching. One is the use of multimode elements to achieve wide angle scan compensation. The other deals with bandwidth limits posed by not having true time delay phase shifters in a phased array. It is found for scans out to $\pm 60^\circ$ on allowing a 0.7 db gain loss that the array beamwidth in degrees is approximately equal to the array bandwidth (%) for cw operation.

Chapter III contains the development and utilization of a computer simulation of a planar phased array of circular waveguide elements. The simulation allows experimental work to be done on the computer and is directed toward the investigation of mutual coupling and wide angle impedance matching in phased arrays. Special emphasis is given to circular polarization. The aforementioned computer program has as variable inputs: frequency, polarization, grid geometry, element size, dielectric waveguide fill, dielectric plugs in the waveguide for impedance matching, and dielectric sheets covering the array surface for the purpose of wide angle impedance matching. Parameter combinations were found which produced reflection peaks interior to grating lobes, while dielectric cover sheets were successfully employed to extend the usable scan range of a phased array. The most exciting results came from the application of computer-aided optimization techniques to the design of this type of array. Different combinations of parameters were allowed to vary and several optimizations were found. As a consequence of the many separate investigations made possible by this program, some fairly general conclusions regarding polarization and WAIM effects could be made, and these are summarized in Chapter III.

The last chapter gives a brief description of some of the experimental work done during the course of this study. Of importance to the above was the design and construction of a waveguide simulator [8] which was used to test the accuracy of the computer simulation for the array of circular waveguides.

CHAPTER II

SUPPLEMENTARY PHASED ARRAY DESIGN CONSIDERATIONS

In this chapter some topics are covered which are not included in other reports, yet are pertinent to wide angle impedance matching (WAIM) considerations in phased arrays. A brief survey and comparison of some of the major WAIM methods is presented below and later sections in this chapter are devoted to discussions of multimode elements for scan matching and bandwidth limitations in phased arrays.

A. Methods for Wide Angle Impedance Matching - Comparison

Two of the main objectives of this project were to determine design procedures for the various WAIM methods and to extend WAIM techniques to the matching problems associated with circularly polarized antenna elements. A thorough coverage of the theory and design practices for most of the WAIM methods is found in Technical Report No. 1 [1] while Chapter III of this report contains an exhaustive study of wide angle scan improvement methods with circularly polarized elements. The analysis in Chapter III is for array elements described by circular apertures, cylindrical cavities or circular waveguides. A treatment of the simpler analytic case of rectangular waveguides used for circular polarization is given in a recent article by Lee [9]. Technical Report No. 3 contains an investigation of Archimedian spirals. The above three works well represent the types of flush mounted elements commonly used for circularly polarized array elements.

Briefly the principal methods for wide angle impedance matching are:

1. Magill and Wheeler dielectric cover sheet [2]: Here a dielectric slab with a high permittivity is placed over an array surface, and a height, thickness, and dielectric constant combination is sought which will provide WAIM. This method is inexpensive, lends itself nicely to all forms of investigation (waveguide simulators, computer simulation, and experimental coupling or impedance measurements), and as is shown in Chapter III is useful for matching arrays with either linearly or circularly polarized elements. Its only drawbacks are that matches usually are not ideal and bad parameter choices can worsen match rather than improve it.

2. Edelberg and Oliner fences and baffles [11]:

Metal fences or baffles or posts are placed on an array surface in order to reduce deleterious mutual coupling effects. In practice metal fences were used to reduce E plane scan variations in an array of $\lambda/2$ dipoles. An array with a VSWR of ≤ 2.9 out to a 60° scan angle had, after adding such fences, a VSWR ≤ 1.6 [10]. In general this method relies on experimental trial and error. Also the surface modifications are not flush mounted and can contribute to shadowing which limits the potential scan range for the array.

3. Interconnecting circuit method of Hannan, Lerner, and Knittel [3]:

This method places reactive networks between adjacent element feed lines in an array. The interconnecting reactances produce an equivalent

reactance to ground which varies with scan angle and can be used to counteract variations in element impedance with scan caused by mutual coupling. Technical Report No. 2 [5] contains an extensive discussion of this method. Its main problem is that it is very difficult to implement.

4. Multimode elements:

These are discussed later in this chapter. If the weight of waveguide elements can be tolerated, this type of element is a good approach for scans out to 60° . They can be adjusted to impedance match the feed lines, are fairly broadband, and incorporate the means for WAIM into the element itself. They operate by generating higher order propagation waveguide modes which can be adjusted to cancel out reflections from the aperture. The mutual coupling between elements for the various higher order modes tends to average out to give a wide matched scan. The concept might be usefully applied to other element types.

5. Use of many closely spaced elements:

This type of system can result in wide angle impedance match, however, it suffers from two disadvantages. First the additional number of elements needed to fill the array add unnecessary cost compared to other matching schemes that can achieve the same match using the minimal number of elements. Finally very small cavity or waveguide-like elements are difficult to match to free space.

6. Electronically tunable matching networks: This is a futuristic approach which is presently expensive and subject to failure when components fail.

B. Multimode Array Elements for Wide Angle Scans

Wong et al. [4] have by generating higher order modes in elements for phased arrays achieved a novel method for controlling mutual coupling so as to maintain a nearly uniform driving point impedance over a specified scan range. Using rectangular waveguide elements enough propagating modes are generated (usually TE_{10} , TE_{20} , and TE_{30}) and then adjusted to produce a cancellation in the net reflected field from the radiating aperture. The higher order modes are generated in waveguide inserts using discontinuities. These higher order modes accomplish two purposes. First the inserts can be adjusted to match the waveguide to the aperture radiating into free space (a broadside match is normally sought). The second is a consequent side-effect which often improves wide angle scan performance. Qualitatively this results from the fact that the net mutual coupling impedance between a reference element and all the other elements in

the array now depends on several different modes whose changes with scan angle tend to offset one another, thereby maintaining a constant Z_{in} over wider scans.

Several methods for generating the higher order waveguide modes are illustrated in Fig. 2-1. The two principal generating schemes suggested are discussed below.

1. Guides are filled with a dielectric slab and a discontinuity is positioned to produce TE_{20} and TE_{30} modes in addition to the TE_{10} mode already present. A cylindrical hole is useful for such mode excitation. The length of the slab and the location of the holes are varied to obtain the relative magnitudes and phases of each mode necessary for matching. Waveguide simulations and computer simulations were used for initial designs, and at Hughes Aircraft [4] a 256 element, linearly polarized array of rectangular waveguide elements was built. The Hughes array had an input VSWR ≤ 1.5 for scan out to $\pm 47^\circ$ in E, H, and D planes. The VSWR was less than 2.5 for 60° scans. The

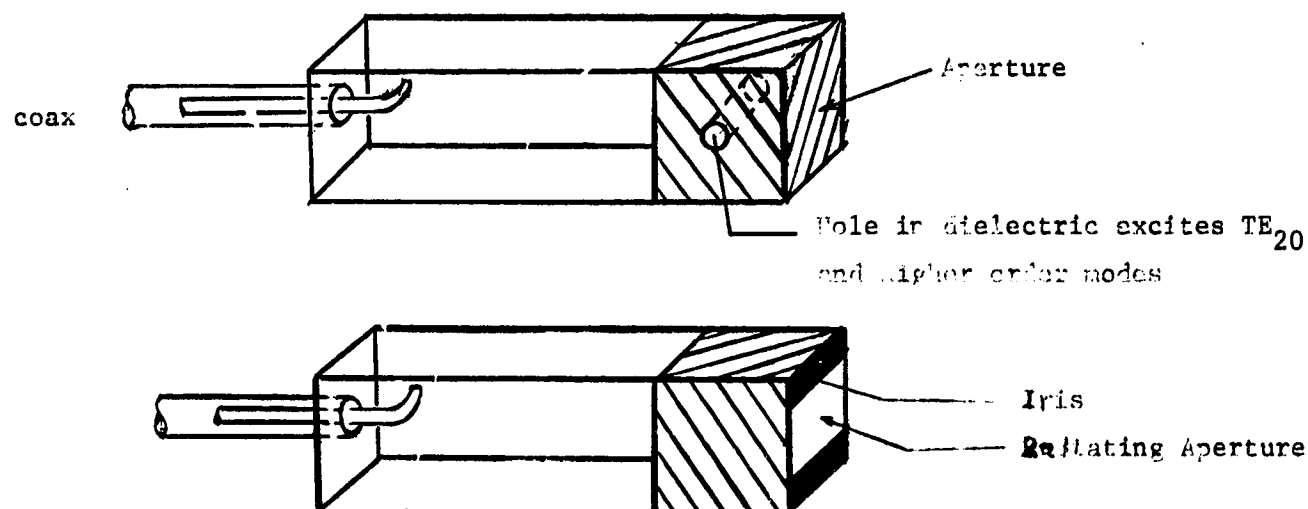


Fig. 2-1. Multimode Waveguide Elements Realization.

major problem with the hole-in-dielectric type of element is one of bandwidth. Since the relative hole position changes with frequency, the mode balance is upset and the element is frequency sensitive.

2. Inductive rises at the interface between waveguides and free space are capable of producing a wideband, multimode element. The size of an iris is found to be fairly effective in controlling the relative proportions of the higher order modes for match. In addition, no critical distances are involved and thus the element has good frequency response characteristics. Arrays of such elements with a 20% bandwidth out to $\pm 53^\circ$ with a VSWR ≤ 1.7 have been built and tested [4].

C. Bandwidth Considerations in Phased Arrays

Whether or not bandwidth is part of the design problem in phased arrays depends on the system objectives and on the frequency ranges used. For instance a 1% bandwidth about a 18 GHz carrier gives a 180 MHz channel while at 3 GHz the channel would be limited to 30 MHz (which is still adequate for many applications). The factors influencing bandwidth are array aperture effects, the array feed system, the type of phase shifters, and component or receiver bandwidths. From a noise point of view it is often advantageous to let the antenna do the prefiltering for a receiver in which case narrow array bandwidths could be a desired asset. Emphasis in this section is on bandwidth limitations related to array apertures and feeds for arrays which are characterized by equal feed line lengths and fixed phase shifters. As a consequence of the fixed phase shifters, the array beam scans with frequency causing a loss in gain relative to the gain

expected for a given scan direction. Note that an array using true time delay phase shifters would not scan with frequency and would have an infinite array bandwidth. The bandwidth of true time delay system would be set by the receiver or individual components.

For the fixed phase shifter array Frank and Cheston [29] arrive at the following easily remembered approximation for array bandwidth:

1. For CW operation, a 60° maximum scan, and a 0.7 db allowed gain degradation

$$\text{Bandwidth (\%)} \approx \text{Broadside beamwidth (degrees)}$$

2. For pulse applications

$$\text{Bandwidth (\%)} \approx 2 \times \text{Broadside beamwidth (degrees)}$$

Two examples of this type of feed and phase shifter arrangement, the parallel feed and a modified corporate feed are illustrated in Fig. 2-2. The phase shifter in the corporate feed have been placed so that 0-360° phase shifters can be used without needing to drop multiples of 360° from element phasing.

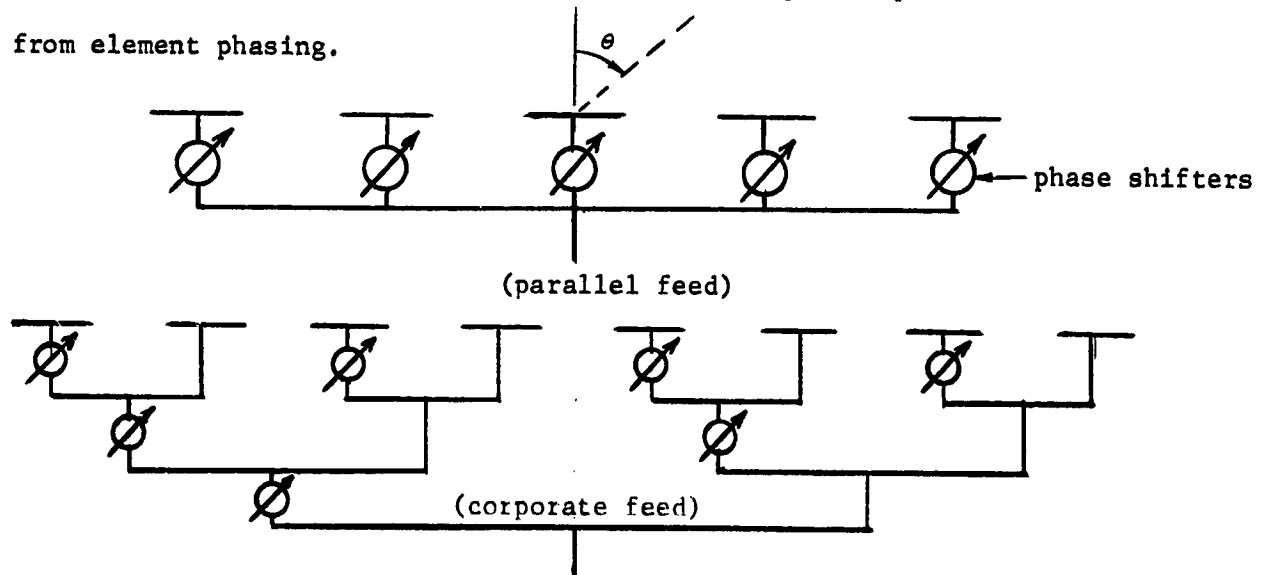


Fig. 2-2. Array Feeds

For linear arrays such as shown in Fig. 2-2 the incremental phase shift between adjacent elements needed to steer the beam in the θ_0 direction is

$$\delta = kd \sin\theta_0 = \frac{2\pi f_1 d}{c} \sin\theta_0 \quad (2-1)$$

where

$$\psi = kd \sin\theta - \delta \text{ and } f_1 \text{ is the center frequency.}$$

Providing the phase shifter settings remain constant, then at a new frequency f_2 the beam is steered to the direction $\theta_0 + \Delta\theta$ giving

$$\delta = \frac{2\pi f_1 d}{c} \sin\theta_0 = \frac{2\pi f_2 d}{c} \sin(\theta_0 + \Delta\theta) \quad (2-2)$$

For $\Delta\theta$ small, $\sin(\theta_0 + \Delta\theta) \approx \sin\theta_0 + \Delta\theta \cos\theta_0$. Substituting in the above

$$\frac{2\pi f_1 d}{c} \sin\theta_0 \approx \frac{2\pi d f_2}{c} (\sin\theta_0 + \Delta\theta \cos\theta_0) \quad (2-3)$$

and solving for $\Delta\theta$ yields

$$\Delta\theta \approx \frac{f_1 - f_2}{f_2} \tan\theta_0 \text{ (radians).} \quad (2-4)$$

From the above it is seen that for f_2 greater than f_1 the beam is scanned toward broadside, while for f_2 less than f_1 the beam swings away from broadside. Further, when the beam is pointed toward broadside $\tan\theta_0 = 0$, and hence the beam does not scan with frequency (bandwidth infinite).

Additional simplifications result by assuming a small percentage bandwidth. Writing

$$f_2 = f_1 \mp \Delta f \quad (2-5)$$

it follows that

$$\bar{f} \Delta\theta = \frac{f_1 - (f_1 + \Delta f)}{f_1 + \Delta f} \tan\theta_0 \approx \bar{f} \frac{\Delta f \tan\theta_0}{f_1} \quad (2-6)$$

or

$$\Delta\theta \text{ (radians)} \approx \frac{BW(\%)}{200} \tan\theta_0 \quad (2-7)$$

where

$BW = 2\Delta f = \text{bandwidth}$

$\Delta\theta = \text{scan deviation from band center.}$

In degrees Eq. 2-7 becomes

$$\Delta\theta(\text{degrees}) = .287 BW(\%) \tan\theta_0 \quad (2-8)$$

Frank and Cheston define a bandwidth factor

$$K = \text{bandwidth factor} = \frac{\text{bandwidth}(\%)}{\text{broadside beamwidth (degrees)}} \quad (2-9)$$

and normalize (2-8) to

$$\frac{\Delta\theta}{\theta_B(\text{scanned})} \approx 0.287 K \sin\theta_0 \quad (2-10)$$

by introducing the large array approximation

$$\theta_B(\text{scanned}) = \text{beamwidth at } \theta_0 = \frac{\theta_B(\text{broadside})}{\cos\theta_0} \quad (2-11)$$

For a maximum gain loss of 0.7 db the bandwidth must be such that the beam never scans more than $\pm 1/4$ the local beamwidth and hence

$$\left| \frac{\Delta\theta}{\theta_B(\text{scanned})} \right| \leq 1/4 \quad (2-12)$$

Applying this condition to Eq. 2-10 gives

$$K_{\max} = \frac{0.87}{\sin \theta_0} \quad (2-13)$$

For an array designed of a maximum scan of 60°

$$K_{\max} = \frac{.87}{\sin 60^\circ} \approx 1$$

Thus the worst case for a 60° from broadside scan is

$$BW(\%) = \theta_B(\text{broadside}) = \text{broadside beamwidth (degrees)} \quad (2-14)$$

A similar procedure working in terms of "equivalent pulse length" results in

$$\text{pulse length} \approx 2 \times \text{aperture size}$$

and

$$\text{bandwidth } (\%) \approx 2 \times \text{broadside beamwidth (degrees)}$$

CHAPTER III

CIRCULAR WAVEGUIDE ARRAYS

The main concern of this report is with antenna elements capable of producing circular polarization in a phased array environment and specifically with the mutual coupling and driving point impedance variations with scan angle which can lead to severe power and array efficiency losses as the array is scanned away from broadside. Methods exist for wide angle impedance matching, but most of them require quantitative knowledge of the behavior of array coupling with scan in order to be applied. In this chapter analytical results and an effective digital computer simulation are developed which are valid for an infinite planar array of circular waveguide antennas, an important class of radiating elements useful for circular polarization. Using this simulation WAIM (wide angle impedance matching) methods are employed and computer-aided optimum array designs are determined using Rosenbrock's pattern search method [17]. In addition, these computer phased-array simulations will be used to hopefully resolve the controversy over two seemingly contradictory ways to best achieve WAIM, namely, by using closely spaced large elements with a high degree of mutual coupling or by using small loosely coupled elements.

The following antenna realizations are fairly representative of those used to obtain circular polarization in arrays:

1. Circular waveguides or cavities with or without dielectric covers.
2. Square guides

3. Crossed dipoles (wire, thick, folded, bent).
4. Crossed slots backed with rectangular or circular cavities.
5. Spirals.
6. Wheeler elements [18] each consisting of a circular cavity below cutoff, fed with an internal crossed thick dipole, and having dielectric layers for transmission matching.

Much theoretical and experimental work has already been done on rectangular guide and cavity elements [36-40] and on external dipole arrays [11-16]. However, square and rectangular elements do not pack well in 60° triangular grid arrays which are in standard use because of the savings in number of elements [21], and further the element shapes are such that mutual coupling is apt to be greater in certain regions of an array cell than that found for circular elements. Volumes of data on dipoles are available, yet because dipoles are subject to shadowing with scan and because they require support structures which can interact with the dipole fields, dipole arrays can be more difficult to analytically predict and to achieve wide angle scans. On the other hand, flush mounted circular elements have the following advantages for use in phased arrays [18]:

1. Circular apertures fit into equilateral triangular grids thus requiring the fewest number of elements for wide-angle scans free of grating lobes.
2. Circular apertures are suited for resonant windows having maximum bandwidth for radiation loading.
3. A circular aperture is resonant in the TE_{11} mode.
4. Circular symmetry is suited for linear, crossed-linear, or circular polarizations.
5. Circular symmetry is amenable to realization with waveguide simulators for infinite planar arrays.
6. Circular apertures tend to reduce coupling wave effects.
7. Mechanical strength and simplicity are characteristic.
8. Many circular elements lend themselves to analysis.

9. Flush elements are aerodynamically smooth.

In view of the above, it was decided that practical mutual coupling and efficiency effects in scanned arrays could be studied fruitfully by investigating infinite planar arrays of circular waveguide elements and infinite arrays of planar spirals. Arrays of circular waveguides are treated in this report, while arrays of spirals are examined in Technical Report No. 3 [19]. A diagram of a possible realization for a typical radiator with circular geometry is shown in Fig. 3-1.

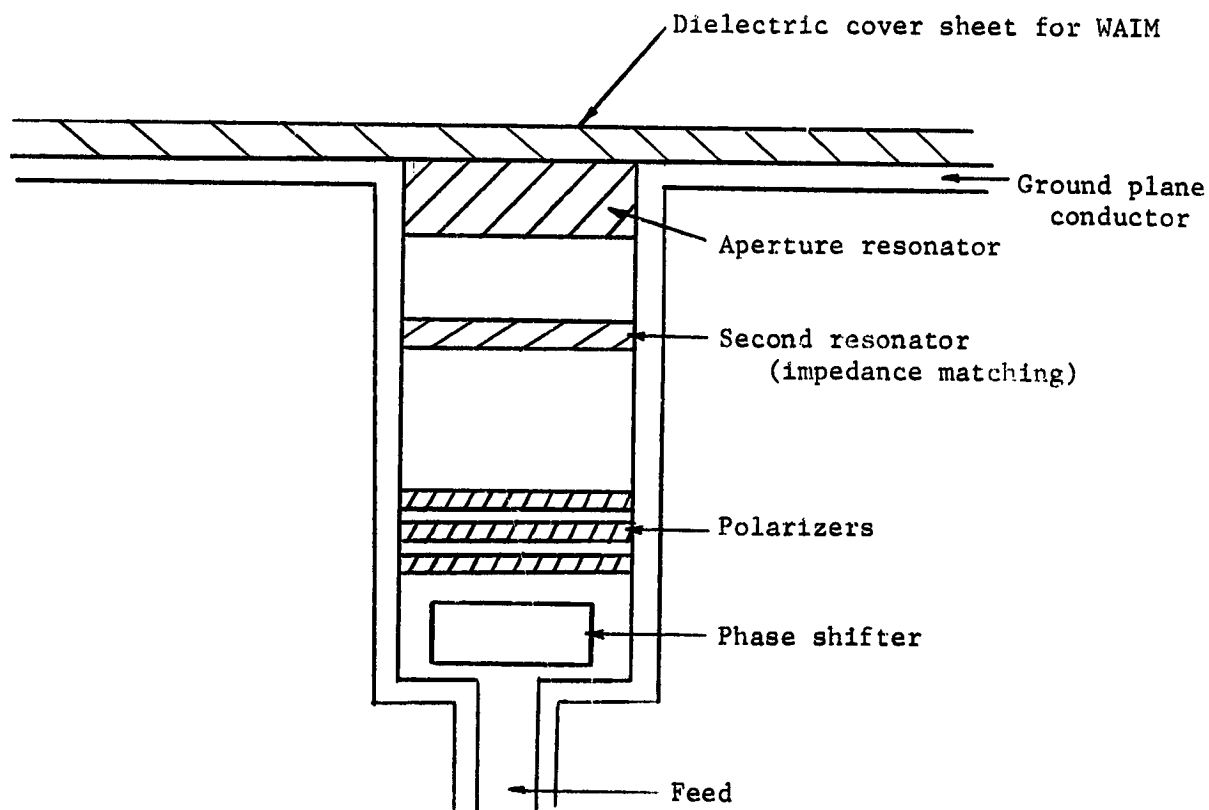


Fig. 3-1 Circular Radiator

As can be seen, the element in Fig.3-1 consists of a circular waveguide with provisions for a feed and dielectric discs (some noncircular) for mode generation and impedance control. The noncircular discs can be used to generate and phase the modes needed to produce an arbitrary polarization, and the circular dielectric discs or "plugs" can be used as resonators to obtain a wideband element or as quarter-wave plates for impedance matching. In any event, circular waveguide systems can be used to investigate a wide class of flush-mounted, circular aperture type sources (the circular cavity and the Wheeler element both easily fit this category). The spiral is a class by itself, and the analysis of both types should further the state of the art and give insight into the optimum design of phased arrays.

A. Computer Simulation of an Infinite Array of Circular Waveguides

An infinite planar array of circular waveguides such as shown in Fig.3-2 has been analyzed and simulated on a digital computer with the following design flexibility:

1. Arbitrary parallelogram grids (α, b, d).
2. Arbitrary dielectric constant in the waveguides (EPS).
3. Dielectric plugs or discs (EPS2, T2) in the waveguides for impedance matching.
4. A dielectric cover sheet (EPS3, T3) over the array face for wide angle impedance matching (WAIM).
5. Scan in any direction (THETA, PHI) or across any scan plane.
6. Arbitrary polarization using crossed TE_{11} waveguide modes.

To solve this complex problem, Harrington's method of moments [7]

or, specifically, the Ritz-Galerkin method is applied to a boundary value formulation of the fields at the interface between the waveguides and free space, and this yields an integral equation that has a well-behaved matrix solution. A time variation of $e^{i\omega t}$ is assumed, and all field quantities are in phasor form. The element locations for an x-y plane grid are

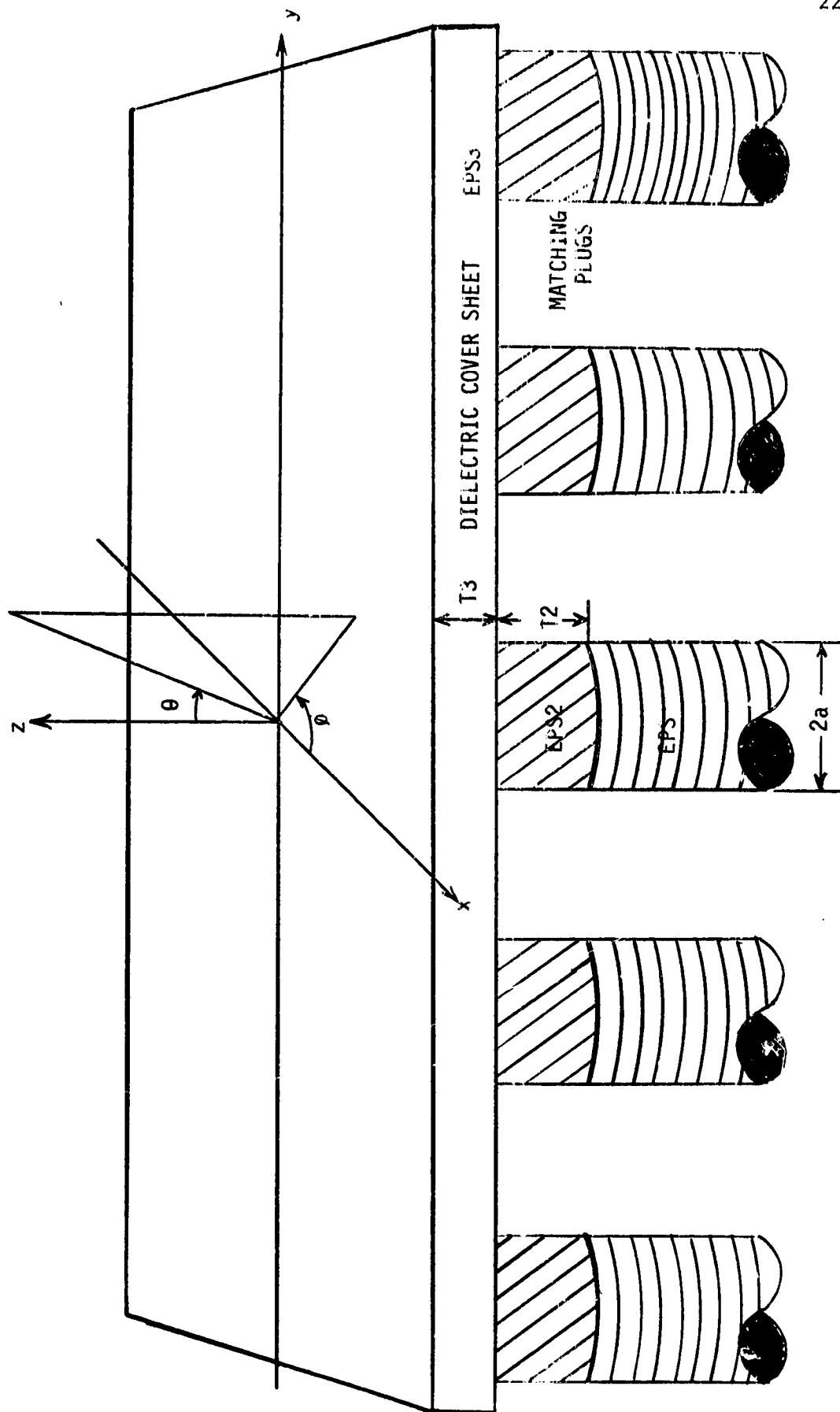


Fig. 3-2 Dielectric Covered Array of Circular Waveguides

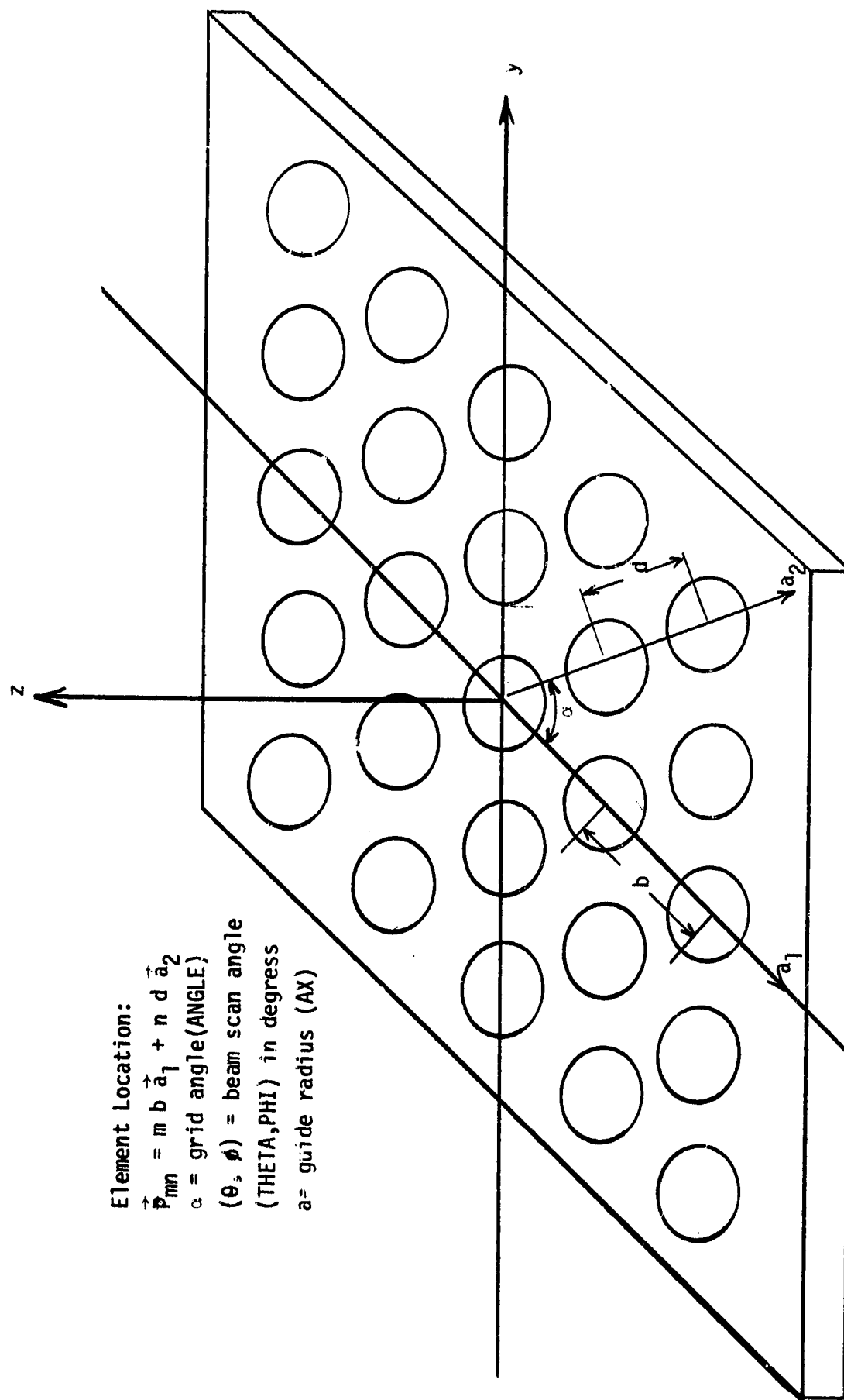


Fig. 3-3 Planar Array Grid Geometry

given by

$$P_{mn} = m b \vec{a}_1 + n d \vec{a}_2 \quad (3-1)$$

as shown in Fig. 3-3 where

b = interelement spacing along the x-direction (BX)

d = element spacing along \vec{a}_2 (D)

α = angle between \vec{a}_1 and \vec{a}_2 = grid angle (ANGLE)

\vec{a}_1, \vec{a}_2 ~ unit vectors

Initially an infinite array of dielectric filled circular waveguide interfaced directly with free space will be analyzed. Once these results are obtained the extensions to allow for dielectric discs in the guides and dielectric cover sheets are straight forward.

I. Waveguide fields (interior region $z \leq 0$)

In this region the solutions can be expressed as the sum of a complete orthonormal sequence of vector modes $\{\vec{\phi}_j e^{\pm \gamma_j z}\}$. Only the transverse field components are considered since when boundary conditions are later applied only the tangential fields are retained. Within the guide the transverse electric field can be expanded

$$\vec{E}_T(\text{int.}) = \sum_{j=1}^J (I_j e^{-\gamma_j z} + R_j e^{+\gamma_j z}) \vec{\phi}_j + \sum_{j=1}^{\infty} R_j e^{\gamma_j z} \vec{\phi}_j \quad (3-2)$$

over the aperture

= 0 over the rest of the cell

where $\{\vec{\phi}_j\}$ account for all TE_{mn} and TM_{mn} modes (vertical and horizontal).

If the propagation constant of the j^{th} mode, $\gamma_j = \alpha_j + i\beta_j$, is purely

imaginary ($\gamma = i\beta_j$), the mode propagates and the guide admittances are given by

$$Y_{TE} = \frac{\beta_j}{k_d} Y_0 = Y_0 \sqrt{1 - \left(\frac{k_c}{k_d}\right)^2} = Y_0 \sqrt{1 - \left(\frac{f_c}{f}\right)^2} = \frac{\gamma}{i\omega\mu} \quad (3-3)$$

$$Y_{TM} = \frac{k_d}{\beta_j} Y_0 = \frac{Y_0}{\sqrt{1 - (k_c/k_d)^2}} = \frac{i\omega\epsilon}{\gamma} \quad (3-4)$$

where $Y_0 = \sqrt{\frac{\epsilon_d}{\mu_d}} = \frac{1}{Z_0}$ and $k_d = \omega \sqrt{\mu_d \epsilon_d}$.

The transverse H-field can be shown to be [20]

$$\vec{H}_T(\text{int.}) = \vec{a}_z \times \sum_m (Y_m I_m e^{-ik_m z} - Y_m R_m e^{+ik_m z}) \vec{\phi}_m \quad (3-5)$$

2. Exterior Fields ($z \geq 0$)

For the region above the waveguides Floquet type modes [20,28] can be used to describe the fields, and for a doubly periodic planar grid the resultant sequence of expansion vectors are called Bloch functions $\{\vec{\psi}_{mnp} e^{\frac{+iB_{mnp}}{2\pi} z}\}$. Expanding the electric field over a grid cell in terms of these vectors yields

$$\vec{E}(\text{ext.}) = \sum_{p=1}^2 \sum_m \sum_n D_{mnp} \vec{\psi}_{mnp} \quad (3-6)$$

where $p = 1$ denotes the TE modes

$p = 2$ denotes the TM modes.

The H-field is accordingly

$$\bar{H}(\text{ext.}) = \vec{a}_z \times \sum_{p=1}^2 \sum_m \sum_n D_{mnp} Y'_{mnp} \psi_{mnp} \quad (3-7)$$

For the above expansion vectors the mode admittances are given by

$$Y'_{mn1} = Y'_{mn} (\text{TE}) = \frac{B_{mn}}{\omega\mu} = \frac{B_{mn}}{k_d} Y_0 \quad (3-8)$$

$$Y'_{mn2} = Y_{mn} (\text{TM}) = \frac{\omega\epsilon}{B_{mn}} = \frac{k_d}{B_{mn}} Y_0 \quad (3-9)$$

where

$$Y_0 = \sqrt{\frac{\epsilon}{\mu}} \quad \text{and} \quad k_d = \omega\sqrt{\mu\epsilon}.$$

More details on the waveguide and free space expansion functions are contained in subsequent sections of this chapter.

At the aperture interface between the guide region and free space ($z = 0$), boundary conditions require that tangential \bar{E} and \bar{H} be continuous across the boundary. Hence

$$\bar{E}_{\text{tangential}} = \bar{E}_T(\text{int.}) = \bar{E}_T(\text{ext.}) \text{ over the grid cell} \quad (3-10)$$

$$\bar{H}_{\text{tangential}} = \bar{H}_T(\text{int.}) = \bar{H}_T(\text{ext.}) \text{ over the aperture only} \quad (3-11)$$

The coefficients in the series expansion for \bar{E}_T can be obtained using the orthogonal properties of the mode functions

$$I_j + R_j = \vec{E}(\text{int.}), \quad \vec{\phi}_j = \iint_{\text{aperture}} \vec{E}_T \cdot \vec{\phi}_j \, dA \quad (3-12)$$

$$D_{mnp} = \vec{E}(\text{ext.}), \quad \vec{\psi}_{mnp}^* = \iint_{\text{cell}} \vec{E}_T \cdot \vec{\psi}_{mnp}^* \, dA \quad (3-13)$$

where * denotes complex conjugate. The boundary condition equation for tangential \vec{H} is then manipulated to get an integral equation for tangential E field. From Eqs. (3-5) and (3-7)

$$\begin{aligned} \vec{H}_T(\text{int.}) &= \vec{a}_z \times \sum_j (I_j - R_j) Y_j \vec{\phi}_j \\ &= \vec{H}_T(\text{ext.}) \end{aligned} \quad (3-14)$$

$$\begin{aligned} &= \vec{a}_z \times \sum_p \sum_m \sum_n D_{mnp} Y'_{mnp} \vec{\psi}_{mnp} \\ &= \vec{a}_z \times \sum_p \sum_m \sum_n Y'_{mnp} \vec{\psi}_{mnp} \iint_A \vec{E}_T \cdot \vec{\psi}_{mnp}^* \, da \end{aligned} \quad (3-15)$$

From (3-15)

$$\sum_j (I_j - R_j) Y_j \vec{\phi}_j = \sum_p \sum_m \sum_n Y'_{mnp} \vec{\psi}_{mnp} \iint_A \vec{E}_T \cdot \vec{\psi}_{mnp}^* \, da \quad (3-16)$$

Adding $\sum_j \underbrace{\vec{\phi}_j Y_j \iint_A \vec{E}_T \cdot \vec{\phi}_j^* \, da}_{I_j + R_j}$ to both sides of (3-16) yields

$$\begin{aligned}
2 \sum_j I_j Y_j \vec{\phi}_j &= \sum_{j=1}^{\infty} Y_j \vec{\phi}_j \iint \vec{E}_T \cdot \vec{\phi}_j da \\
&+ \sum_p \sum_m \sum_n Y'_{mnp} \vec{\psi}_{mnp} \iint \vec{E}_T \cdot \vec{\psi}_{mn}^* da
\end{aligned} \quad (3-17)$$

where Eq. (3-17) is an integral equation whose solution or unknown is the tangential E-field, \vec{E}_T .

Substituting (3-1) for \vec{E}_T in (3-17) gives

$$\begin{aligned}
2 \sum_j I_j Y_j \vec{\phi}_j &= \sum_{j=1}^{\infty} (I_j + R_j) Y_j \vec{\phi}_j \\
&+ \sum_p \sum_m \sum_n Y'_{mnp} \vec{\psi}_{mnp} \iint \sum_k (I_k + R_k) \vec{\phi}_k \cdot \vec{\psi}_{mnp}^* da
\end{aligned} \quad (3-18)$$

Taking moments with respect to the set $\{\vec{\phi}_j\}$ [19]

$$\begin{aligned}
2 Y_j I_j &= Y_j (I_j + R_j) \\
&+ \sum_p \sum_m \sum_n Y'_{mnp} \iint \vec{\psi}_{mnp} \cdot \vec{\phi}_j da \iint \sum_k (I_k + R_k) \vec{\phi}_k \cdot \vec{\psi}_{mnp}^* da
\end{aligned} \quad (3-19)$$

The above expressed in matrix form is

$$2 \begin{bmatrix} Y_1 I_1 \\ \vdots \\ Y_j I_j \\ \vdots \\ 0 \\ \vdots \\ 0 \end{bmatrix} = \begin{bmatrix} \vdots \\ A \\ \vdots \end{bmatrix} \begin{bmatrix} I_1 + R_1 \\ I_2 + R_2 \\ \vdots \\ I_j + R_j \\ R_j + 1 \\ \vdots \\ R_N \end{bmatrix} \quad (3-20)$$

where

$A = (a_{ji})$ matrix with elements a_{ji}

$$a_{ji} = Y_j \delta_{ji} + \sum_p \sum_m \sum_n Y'_{mnp} C_{mnpj} C_{mnp1}^* \quad (3-21)$$

$$C_{mnpj} = \iint_{A_p} \vec{\phi}_j \cdot \vec{\psi}_{mnp} da = \text{mode coupling coefficient} \\ \text{(interior to exterior)} \quad (3-22)$$

I_j = input = complex component of $\vec{\phi}_j$ guide mode
incident at the aperture

R_j = reflected component of $\vec{\phi}_j$ mode

Y_j = characteristic admittance of j^{th} waveguide mode

Y_{mnp} = characteristic admittance of radiation modes .

Inverting the above matrix equation gives

$$\begin{bmatrix} I_1 + R_1 \\ \vdots \\ I_j + R_j \\ \vdots \\ R_N \end{bmatrix} = A^{-1} \begin{bmatrix} 2Y_1 I_1 \\ \vdots \\ 2Y_j I_j \\ \vdots \\ 0 \end{bmatrix} \quad (3-23)$$

where

A^{-1} = inverse of $A = (a_{mn}^I)$

a_{mn}^I = element of the inverted A matrix.

The inverse can be determined on a digital computer provided the elements, a_{mn}^I , of the A matrix can be found and the matrix is nonsingular. A discussion of convergence and truncation effects in mode coupling solutions

of this nature can be found in Lee et al. [24] and Mittra [25]. In this solution K_{\max} and L_{\max} which determine the number of free space modes were allowed to vary together and independently from 7 to 29. No solution oscillation or divergence problems were observed, and since the numerical results also agreed with the waveguide simulator measurements of Amitay and Galindo [22], accuracy was judged to be good. For many problems $K_{\max} = L_{\max} = 13$ was used.

3. Coupling Coefficients

The key to practical realizations of this problem on a computer is that the coupling coefficients, C_{mnpj} , can be evaluated analytically. As a consequence, it is unnecessary to rely on time consuming (integration time even on a high speed machine such as a Univac 1108 would have been considerable), expensive, and accuracy limiting numerical integration techniques. In addition, having analytic formulations of these waveguide to free space mode coupling coefficients, it is possible to better consider the number of free space modes needed to achieve reasonable convergence of the series for each of the A matrix elements.

For circular waveguide apertures

$$C_{rspj} = \int \int_{\text{aperture}} \vec{\phi}_j \cdot \vec{\psi}_{rsp} da = \int_0^a \int_0^{2\pi} \phi_j \cdot \vec{\psi}_{rsp} r d\phi dr \quad (3-24)$$

where

$p = 1$ denotes TE waves

$p = 2$ denotes TM waves.

The waveguide modes $\{\vec{\phi}_j\}$ are actually more complex in that (j) depends on the mode being TM or TE, vertical or horizontal, and marked by a two-dimensional wavenumber. Hence, in evaluating the coupling coefficients,

it is helpful to utilize a subscript and superscript notation

$$C_{rs,j}^p = C_{rs,mn}^{p,q}$$

Substituting for $\vec{\phi}_j$ and $\vec{\psi}_{rs}$ in (3-24) and performing the weighty task of integration, it can be shown

$$\begin{matrix} V \\ H \end{matrix} \left\langle \vec{\phi}_{mn}(\text{TE}), \vec{\psi}_{rs}(\text{TE}) \right\rangle = \frac{2\pi\lambda_{mn} i^{m-1}}{k_r^2(r,s) - \lambda_{mn}^2} a J_m(\lambda_{mn} a) J_m'(k_r a) \begin{pmatrix} \cos m \psi \\ \sin m \psi \end{pmatrix} \quad (3-25)$$

$$\begin{matrix} V \\ H \end{matrix} \left\langle \vec{\phi}_{mn}(\text{TM}), \vec{\psi}_{rs}(\text{TM}) \right\rangle = \frac{2\pi\lambda_{mn} i^{m-1}}{k_r^2 - \lambda_{mn}^2} (-k_r) J_m'(\lambda_{mn} a) J_m(k_r a) \begin{pmatrix} \sin m \psi \\ \cos m \psi \end{pmatrix} \quad (3-26)$$

$$\begin{matrix} V \\ H \end{matrix} \left\langle \vec{\phi}_{mn}(\text{TE}), \vec{\psi}_{rs}(\text{TM}) \right\rangle = \frac{2\pi m}{k_r} i^{m-1} J_m(\lambda_{mn} a) J_m(k_r a) \begin{pmatrix} \sin m \psi \\ -\cos m \psi \end{pmatrix} \quad (3-27)$$

$$\begin{matrix} V \\ H \end{matrix} \left\langle \vec{\phi}_{mn}(\text{TM}), \vec{\psi}_{rs}(\text{TE}) \right\rangle = 0 \quad (3-28)$$

where

$$\psi = \text{PSI} = \tan^{-1} \frac{k_y}{k_x} \quad (3-29)$$

V denotes vertical

H denotes horizontal.

Converting the above to the subscript and superscript notation

$$C_{rs,mn}^{1,2} = 0 \quad (3-30)$$

$$C_{rs,mn}^{1,1} = \frac{2\pi\lambda_{mn}^2 i^{m-1}}{k_r^2(r,s) - \lambda_{mn}^2} a J_m(\lambda_{mn} a) J_m'(k_r a) \begin{pmatrix} \cos m \psi \\ \sin m \psi \end{pmatrix} \begin{matrix} V \\ H \end{matrix} \quad (3-31)$$

$$C_{rs,mn}^2 \begin{matrix} 1 \\ -\cos m \psi \end{matrix} = \frac{2\pi m i^{m-1}}{k_r} J_m(\lambda_{mn} a) J_m(k_r a) \begin{matrix} \sin m \psi \\ V \end{matrix} \quad (3-32)$$

$$C_{rs,mn}^2 \begin{matrix} 2 \\ \cos m \psi \end{matrix} = \frac{-2\pi \lambda_{mn}' i^{m-1} k_r}{k_r^2 - \lambda_{mn}'^2} J_m'(\lambda_{mn}' a) J_m(k_r a) \begin{matrix} \sin m \psi \\ V \\ \cos m \psi \\ H \end{matrix} \quad (3-33)$$

Again, the ability to evaluate these coupling coefficients without numerically integrating makes this an extremely effective method. In our computer simulation twenty-two waveguide modes were used, and the resultant mode index (j) and eigenvalue for each type of mode are listed in Table I below. Note that the index (j) lumps information as to whether the mode is TE_{mn} or TM_{mn} and vertical or horizontal into a single index.

Table I Waveguide Mode Ordering

j	Φ_j mode	eigenvalues
1	$TE_{11}(V)$	1.87
2	$TE_{11}(H)$	
3	$TM_{11}(V)$	3.83
4	$TM_{11}(H)$	
5.	$TE_{21}(V)$	3.05
6	$TE_{21}(H)$	
7	$TM_{21}(V)$	5.13
8	$TM_{21}(H)$	
9	$TE_{31}(V)$	4.2
10	$TE_{31}(H)$	
11	$TM_{31}(V)$	6.38
12	$TM_{31}(H)$	
13	$TE_{12}(V)$	5.33

Table I (Continued)

j	ϕ_j mode	eigenvalues
14	TE ₁₂ (H)	
15	TM ₁₂ (V)	7.015
16	TM ₁₂ (H)	
17	TE ₀₁ (V)	3.83
18	TE ₄₁ (H)	5.31
19	TM ₀₁ (H)	2.4
20	TM ₀₂ (H)	5.52
21	TE ₄₁ (V)	5.31
22	TE ₀₂ (V)	7.015

For most of the array configurations analyzed using this program simulation, the waveguide dimensions were chosen so that only the modes ϕ_1 and ϕ_2 propagate, and hence twenty-two modes should be adequate since twenty of them are below cutoff.

B. Dielectric Cover Sheets and Matching Plugs

As has already been stated, dielectric discs within the waveguide can be used to generate modes or to impedance match between the guide fields and free space. For this purpose dielectric plugs in the ends of the waveguides will be considered. The program modification is simple in that it is only necessary to replace Y_j in (14) by \tilde{Y}_j , the effective waveguide admittance at the $z = 0$ plane looking in the $-z$ direction. Using waveguide and transmission line concepts \tilde{Y}_j is seen to be

$$Y_J = y_{\text{plug}}(J) \frac{y_{\text{guide}}(J) + i y_{\text{plug}}(J) \tan[k_{\text{plug}}(J) * T2]}{y_{\text{plug}}(J) + i y_{\text{guide}}(J) * \tan[k_{\text{plug}}(J) * T2]} \quad (3-34)$$

where

$y_{\text{plug}}(J)$ = characteristic admittance of the ϕ_J mode in the plugs

$y_{\text{guide}}(j)$ = characteristic admittance of the J^{th} mode in the
guide (allows for dielectric fill, EPS)

$k_{\text{plug}}(J)$ = phase constant of the J^{th} mode in the plugs = $-i\gamma$

$T2$ = plug thickness ,

Two dielectric cover sheets are included in the program and should provide a fairly flexible basis for extending the impedance matched scan range of an array. The behavior of the fields in dielectric layers in the region $z \geq 0$ is at first not as obvious as that for the waveguide region. However, the fields in each of the layers and free space can be decomposed into TE and TM waves with respect to z [26], and then normal traveling wave techniques can be used to obtain the modifications of (3-19) needed to solve the problem.

First, recall for systems with both electric and magnetic sources that the total fields are given by

$$\vec{E} = \vec{E}_A + \vec{E}_F = -j\omega\vec{A} - \frac{j\omega}{k^2} \nabla(\nabla \cdot \vec{A}) - \frac{1}{\epsilon} \nabla \times \vec{F} \quad (3-35)$$

$$\vec{H} = \vec{H}_A + \vec{H}_F = -j\omega\vec{F} - \frac{j\omega}{k^2} \nabla(\nabla \cdot \vec{F}) + \frac{1}{\mu} \nabla \times \vec{A} \quad (3-36)$$

Waves propagating TM and TE to z can be determined from

$$\vec{A} = \vec{a}_z \psi^a \quad (3-37)$$

$$\vec{F} = \vec{a}_z \psi^f \quad (3-38)$$

where

ψ^a = magnetic potential

ψ^f = electric potential.

For this case Eqs. (3-35) and (3-36) simplify to [26,27]

$$\vec{E} = -\nabla \times (\vec{a}_z \psi^f) + \frac{1}{i\omega\epsilon} \nabla \times [\nabla \times (\vec{a}_z \psi^a)] \quad (3-39)$$

$$\vec{H} = \nabla \times (\vec{a}_z \psi^a) + \frac{1}{i\omega\mu} \nabla \times [\nabla \times (\vec{a}_z \psi^f)] \quad (3-40)$$

The potential functions are solutions of the homogeneous phasor wave equation (Helmholtz equation) subject to boundary conditions. Above each cell in an infinite array of the type being considered the application of boundary conditions gives separation constants k_x and k_y which are determined by the cell geometry (size and shape) and are not affected by the presence of the dielectric layers. Only k_z depends on the dielectric constant of a layer.

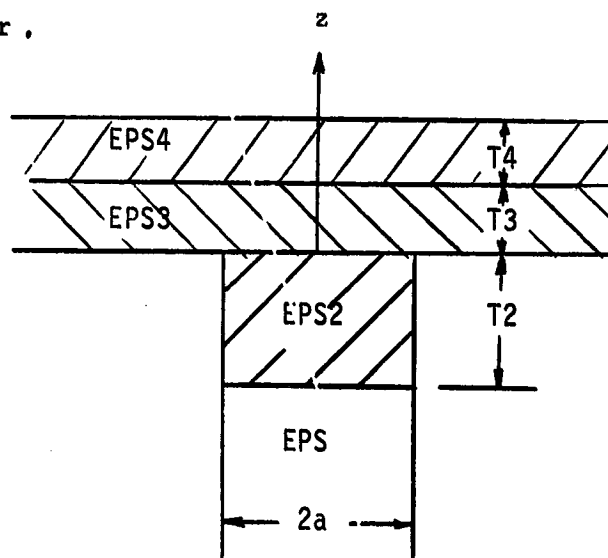


Fig. 3-4. Array Covered with Two Dielectric Sheets.

The solution to the Helmholtz equation for the free space region
 $(z \geq T_3 + T_4)$ is

$$\begin{pmatrix} \psi^a \\ \psi^f \end{pmatrix} = \sum_p \sum_q \begin{pmatrix} D'_{pq} \\ \frac{D_{pq}}{z_o} \end{pmatrix} e^{-1[k_x(p)x + k_y(p,q)y + k_z(p,q)z]} \quad (3-41)$$

where

$$k_x(p) = k_o \sin \theta_o \cos \phi_o + \frac{2\pi p}{b}$$

$$k_y(p,q) = k_o \sin \theta_o \sin \phi_o + \frac{2\pi q}{d \sin \alpha} - \frac{2\pi p}{b \tan \alpha}$$

$$k_z^2(p,q) = k_o^2 - k_x^2 - k_y^2$$

The separation phase constants k_x and k_y are unchanged in a dielectric layer, however, k_z becomes

$$k_z^m(p,q) = \sqrt{k_o^2 \epsilon_m - k_x^2 - k_y^2} \quad (3-42)$$

ϵ_m = relative dielectric constant of the m^{th} layer.

Thus it is seen that the system for $z \geq 0$ can be treated as a cascaded waveguide-like system each section of which is characterized by a wave number, k_z .

1. Single Cover Layer (EPS3, T3)

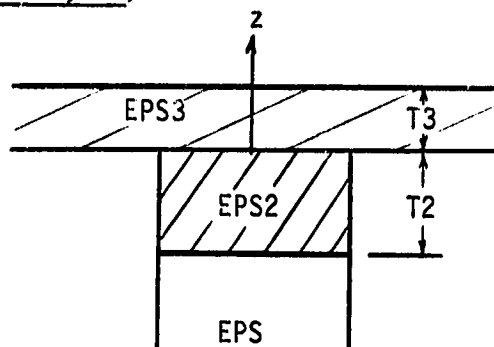


Fig. 3-5. Array Covered with a Single Dielectric Sheet.

For a single layer of dielectric covering the array surface, the admittance at the $z = 0$ plane is

$$Y_{+z}(p,q) = y_3(p,q) \frac{y_o(p,q) + i y_3(p,q) \tan[k_{z3}(p,q) * T3]}{y_3(p,q) + i y_o(p,q) \tan[k_{z3}(p,q) * T3]} \quad (3-43)$$

where

$y_3(p,q)$ = characteristic admittance of the $\vec{\psi}_{pq}^r$ mode in the dielectric layer ($0 \leq z \leq T3$)

$y_o(p,q)$ = free space admittance of the pqr mode ($z > T3$)

$k_{z3}(p,q)$ = wave number of the pq^{th} mode in the dielectric

$T3$ = dielectric thickness

$EPS3$ = relative dielectric constant of the cover sheet.

2. Two Cover Layers (EPS3, T3, EPS4, T4)

In this instance, the admittance looking in the $+z$ direction at the level $z = T3$ is

$$Y_{T3} = Y_{T3}(p,q,r) = y_4(p,q,r) \frac{y_o(p,q,r) + i y_4(p,q,r) \tan[k_{z4} * T4]}{y_4(p,q,r) + i y_o(p,q,r) \tan[k_{z4} * T4]} \quad (3-44)$$

Using the above as the load for the first layer the required admittance at $z = 0$ is

$$Y_{+z}(p,q,r) = y_3(p,q,r) \frac{Y_{T3} + i y_3(p,q,r) \tan[k_{z3} * T3]}{y_3(p,q,r) + i Y_{T3} \tan[k_{z3} * T3]} \quad (3-46)$$

In the above equations

$$y_o(p,q,1) = y_o^{TE}(p,q) = \frac{k_{zo}(p,q)}{\omega \mu_o} = \frac{k_{zo}(p,q) Y_o}{k_o} \quad (3-47)$$

$$y_o(p,q,2) = y_o^{TM}(p,q) = \frac{\omega \epsilon_o}{k_{zo}(p,q)} = \frac{y_o k_o}{k_{zo}(p,q)} \quad (3-48)$$

$$\begin{aligned} k_{zo}^2(p,q) &= k_o^2 \left[1 - \left(\frac{k_x}{k_o} \right)^2 - \left(\frac{k_y}{k_o} \right)^2 \right] \\ &= k_o^2 \left[1 - \left(T_x - \frac{2\pi p}{k b} \right)^2 - \left(T_y - \frac{2\pi q}{k d \sin \alpha} + \frac{2\pi p}{k b \tan \alpha} \right)^2 \right] \end{aligned} \quad (3-49)$$

with k_o being replaced by $k = \omega \sqrt{\mu \epsilon} = k_o \sqrt{\mu_d \epsilon_d}$ to convert to the forms valid for the dielectrics.

C. Waveguide Vector Modes (a = waveguide radius)

For reference purposes this and the next section contain the equations defining the modes used in expanding the waveguide and free-space fields. In a circular waveguide of radius "a" the TE and TM (to z) vector modes are given by

$$\begin{aligned} \vec{V} \\ \vec{H} \end{aligned} \begin{aligned} \vec{\phi}_{mn}(TE) \\ \vec{\phi}_{mn}(TM) \end{aligned} = \hat{a}_r \frac{m}{r} J_m(b_{mn} r) \begin{pmatrix} \sin m\phi \\ -\cos m\phi \end{pmatrix} + \hat{a}_\phi b_{mn} J_m'(b_{mn} r) \begin{pmatrix} \cos m\phi \\ \sin m\phi \end{pmatrix} \quad (3-50)$$

$$\begin{array}{c} V \\ \vec{\phi}_{mn}(TM) = \hat{a}_r (-\alpha_{mn}) J'_m(\alpha_{mn} r) \begin{pmatrix} \sin m\phi \\ \cos m\phi \end{pmatrix} + \hat{a}_r \frac{m}{r} J_m(\alpha_{mn} r) \begin{pmatrix} -\cos m\phi \\ \sin m\phi \end{pmatrix} \\ H \end{array} \quad (3-51)$$

where V denotes the vertical modes (parallel to the y-axis in Fig. 3-3) and H designates the horizontal modes (parallel to the x-axis). Recall that TE modes correspond to roots, b'_{mn} , of

$$\frac{d J_m(b'_{mn} a)}{dr} = 0 \rightarrow \text{roots of } J'_m(\lambda'_{mn}) = 0$$

where $\lambda'_{mn} = b'_{mn} a$.

For TM modes: $J_m(\alpha_{mn} a) = 0 \rightarrow \text{roots } \lambda_{mn} = \alpha_{mn} a$

*Note $TE_{on}(H) = 0$

$TM_{on}(V) = 0$

D. Free Space Wave Functions (Block Functions)

Working with the component of the wave propagating normal to the boundary (z-direction)

$$\vec{\psi}_{(TE)} = \frac{k_y}{k_r} \vec{a}_x - \frac{k_x}{k_r} \vec{a}_y e^{+ik_x x + ik_y y} \quad (3-52)$$

$$\vec{\psi}_{(TM)} = \frac{k_x}{k_r} \vec{a}_x + \frac{k_y}{k_r} \vec{a}_y e^{ik_x x + ik_y y} \quad (3-53)$$

$$k_r^2 = k_x^2 + k_y^2 \quad (3-54)$$

For the mn^{th} mode and a beam pointing direction (θ_o, ϕ_o) the direction cosines are

$$T_x = \sin \theta_o \cos \phi_o \quad (3-55)$$

$$T_y = \sin \theta_o \sin \phi_o \quad (3-56)$$

and

$$k_x(m,n) = k_x(m) = k_o T_x - \frac{2\pi m}{b} \quad (3-57)$$

$$k_y(m,n) = k_o T_y - \left[\frac{2\pi n}{d \sin \alpha} - \frac{2\pi m}{b \tan \alpha} \right] \quad (3-58)$$

α = grid angle

b = spacing along \vec{a}_1 - direction

d = spacing along \vec{a}_2 direction

$$\text{grid points } \vec{p}_{rs} = r b \vec{a}_1 + s d \vec{a}_2$$

To point the beam in the (θ_o, ϕ_o) direction, the differential phase shifts between elements are

$$\delta_x = \frac{2\pi}{\lambda} b T_x = \frac{2\pi}{\lambda} b \sin \theta_o \cos \phi_o \quad (3-59)$$

$$\delta_y = \frac{2\pi}{\lambda} d \sin \alpha T_y = \frac{2\pi}{\lambda} d \sin \theta_o \sin \alpha \sin \phi_o \quad (3-60)$$

For $z \geq 0$ only the forward propagating modes are present (assumes system infinite in which case no reflections occur) and the Floquet modes are $\{\vec{\Psi}_{mnp} e^{-1 \beta_{mn} z}\}$

where

$$\beta_{mn} = \sqrt{k_o^2 - k_r^2}$$

$$\beta_{mn}^2 = k_o^2 \left[1 - \left(\frac{k_x}{k} \right)^2 - \left(\frac{k_y}{k} \right)^2 \right]$$

$$= k^2 \left[1 - \left(T_x - \frac{2\pi m}{bk} \right)^2 - \left(T_y - \frac{2\pi n}{d \sin(\alpha)k} + \frac{2\pi m}{bk \tan \alpha} \right)^2 \right] \quad (3-61)$$

E. Conclusions

Grating lobe predictions are the most commonly used measure for estimating array scan limits, and as such the WAIM attempts in this study are compared with their angular predictions. As expected, it was observed that mutual coupling in physical arrays is such that reflection coefficient peaks can occur interior to the grating lobe angles -- a condition first noted by Farrell and Kuhn[39] and a serious problem in any superficial design. Upon applying WAIM techniques, the reflection coefficient peaks have been moved outside the grating lobe angles thereby extending the usable scan range for a given array geometry. The fact that the grating lobe angle depends on the scan plane chosen is omitted in many discussions of grating lobes, however generalized grating lobe conditions will be developed here because of their need for some of the scan planes investigated. The grating lobe condition for a rectangular grid is [27]

$$\frac{d}{\lambda} = \frac{1}{1 + |\sin \theta_m|} \quad (3-62)$$

which can be rearranged to give

$$\sin \theta_m = \frac{\lambda}{d_m} - 1. \quad (3-63)$$

For equilateral triangular grids the above equation is modified to

$$\frac{d_m}{\lambda} = \frac{1.155}{1 + |\sin \theta_m|}. \quad (3-64)$$

Basically grating lobes appear when the grid points are phased to produce secondary major lobes in visible space. An alternate way of viewing this phenomenon is in terms of the invisible-visible mode

propagation approach. From this point of view, it is seen that grating lobes occur when a secondary free space mode makes the transition from the invisible (nonpropagating or evanescent) to visible region (propagating). The direction cosines of the pointing angle (θ, ϕ) are

$$T_x = \sin \theta \cos \phi \quad (3-65)$$

$$T_y = \sin \theta \sin \phi \quad (3-66)$$

For the free space region exterior to the guides

$$k_x = k_o T_x - \frac{2\pi m}{b}$$

$$k_y = k_o T_y - \frac{2\pi n}{d \sin \alpha} + \frac{2\pi m}{b \tan \alpha}.$$

From the separation equation, the wave numbers for the various free space modes are

$$k_z(m, n) = \sqrt{k^2 - k_x^2(m, n) - k_y^2(m, n)}$$

where

$k_z(0, 0)$ is the desired radiating mode

$k^2 > k_x^2 + k_y^2 \rightarrow$ propagating modes

$k^2 < k_x^2 + k_y^2 \rightarrow$ evanescent modes.

Since grating lobes occur when modes other than the 00^{th} start to propagate, the critical conditions for propagation define the invisible-visible region boundaries. In direction cosine space the boundaries are circles such as shown in Fig. 3-5 and defined by

$$k^2 = k_x^2(m, n) + k_y^2(m, n) = \left(k_o T_x - \frac{2\pi m}{b}\right)^2 + \left(k_o T_y - \frac{2\pi n}{d \sin \alpha} + \frac{2\pi m}{b \tan \alpha}\right)^2 \quad (3-67)$$

Normalized to k_0 (3-67) becomes

$$\epsilon_r \mu_r = \left(T_x - \frac{m\lambda}{b}\right)^2 + \left(T_y - \frac{n\lambda}{d \sin \alpha} + \frac{m\lambda}{b \tan \alpha}\right)^2. \quad (3-68)$$

Grating lobe regions for the grid in Fig. 3-5 are the areas of mutual intersection which are shown shaded.

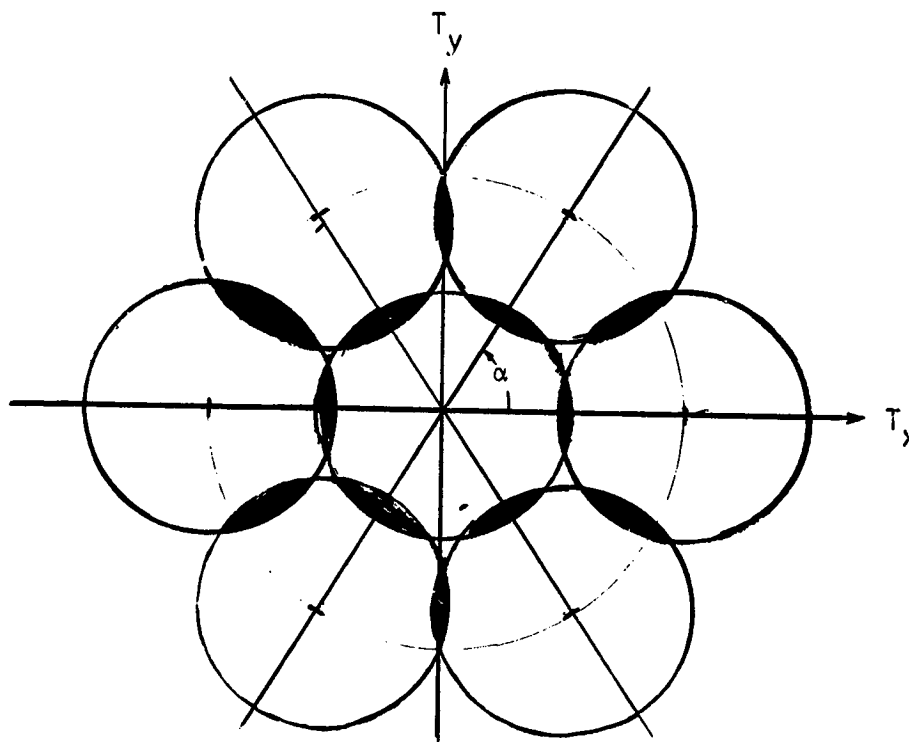


Fig. 3-5 Direction Cosine Space Showing Grating Lobe Regions (60° grid angle)

The following calculations show the determination of grating lobes angles for various scan planes for an equilateral triangular grid array with $b = d = 1.0$ and $\lambda = 1.4$. The incident wave was polarized parallel to the y -axis in the grid plane. The spacings were purposefully chosen to produce a grating lobe in visible space ($\theta = 38^\circ$) so that matching effects could be evaluated, and many of the test programs were run using the 60° scan plane where

cross-polarization effects were found to be significant. The choice of grating lobe angle at $\theta = 38^\circ$ was made in an attempt to somewhat reduce computer time since a scan just beyond the grating lobe angle in a particular plane is all that is usually of interest. Thus by eliminating the necessity of scans to 90° fewer program iterations are used with the resultant savings of computer time. The results of all these simulations are contained in the Appendix.

E-Plane Scan ($\theta = 90^\circ$)

$$k = k_0, d = b = 1.0, \lambda = 1.4, \text{Angle} = 60^\circ$$

For $m = 0$ and $n = 1$, Eq. (3-68) becomes

$$\left(\sin \theta - \frac{\lambda}{d \sin \alpha}\right)^2 = 1$$

$$\sin \theta_{g1} = \frac{\lambda}{d \sin \alpha} \pm 1 = -1 + \frac{1.4}{.8666} = .615$$

$$\theta_{g1} = \sin^{-1} (.615) \approx 38^\circ$$

H-Plane Scan ($\theta = 0^\circ$)

Here the choice $n = 1$ and $n = 0$ is made giving

$$\left(\sin \theta - \frac{\lambda}{b}\right)^2 + \left(\frac{\lambda}{b \tan \alpha}\right)^2 = 1$$

$$\sin \theta - 1.4 = \pm 1 - \left(\frac{1.4}{1.732}\right)^2 = \pm .5893$$

$$\theta_{g1} = 54^\circ$$

60° Scan Plane ($\theta = 60^\circ$) $m = 1, n = 0$

$$\left(\frac{1}{2} \sin \theta - 1.4\right)^2 + \left(\frac{\sqrt{3}}{2} \sin \theta + \frac{1.4}{1.732}\right)^2 = 1.0$$

Solving gives $\theta_{g1} = 54^\circ$ as one would expect since for the hexagonal grid the grid axes could be rotated 60° without changing its structure.

30° Scan Plane ($\theta = 30^\circ$)

From a symmetry consideration similar to the $\theta = 60^\circ$ example

$$\theta_{g1} = 38^\circ .$$

1. Array Performance Observations

In the following I_k is the applied or incident value of the excitation of the k^{th} waveguide mode, and R_k is the reflected component of the k^{th} mode. The complex reflection coefficient for the k^{th} mode is $\Gamma_k = R_k/I_k$. Linear and circular polarizations were obtained by using crossed TE_{11} modes which correspond to modes $\vec{\phi}_1$ and $\vec{\phi}_2$. For most of these examples $\vec{\phi}_1$ and $\vec{\phi}_2$ are the only propagating modes in the waveguides, and hence are of prime interest and will be accordingly emphasized in plots of scan results. Based on many computer experimental simulations [see the Appendix for graphical results], it was observed that

(1) E-plane scans were characterized by the early onset of grating lobe conditions ($\theta_{g1} = 38^\circ$) and probably showed the most intramode reflection coupling I_1 to R_1 .

(2) H-plane scans yielded a grating lobe at $\theta = 54^\circ$ (farthest from broadside for this geometry). Match was fairly good for most configurations out to the grating lobe angle. Generally this was an uninteresting choice of scan plane. This observation should be carefully weighed when considering the use of waveguide simulators

since most simulators are compatible with H-plane scans and thus contribute very little scan information.

(3) The 60° scan plane was characterized by a significant reflected value of the cross-polarized dominant waveguide mode (ϕ_2). The grating lobe was at 54° and the depolarization was found to be greatest near and usually just prior to the grating lobe angle. This scan plane was judged to be the severest test of wide angle matching as a consequence of the cross-polarization effects.

(4) The 30° scan plane had a grating lobe at 38°, but it was subject to less depolarization than the 60° cut. This is still a potentially good scan plane for initial testing.

(5) It was difficult to get reflection peaks interior to the grating lobe angle with an unmodified array of circular waveguide elements in an equilateral triangular grid. The triangular grid and circular elements seem to keep mutual coupling effects to a minimum [34] indicating that this is a seemingly desirable type of element shape and array geometry.

(6) A high degree of coupling of power to higher order evanescent waveguide modes possible. In fact neglect of these modes could lead to some wrong conclusions. A previous study of circular aperture arrays [23] wrongly ignored these effects and also chose to ignore the problem of broadside matching which when the array is actually scanned lead to major design difficulties.

(7) In choosing initial values of dielectric constants and thicknesses the author has proposed some approximate design methods which help in the optimization process [27].

(8) Even though mutual coupling was low for small diameter elements, they were very difficult to match. As a consequence of this difficulty and because of cost and production tolerance considerations at microwave frequencies, larger elements are recommended. The Rosenbrock optimization program was applied with waveguide diameter and dielectric constant as free variables, and the program choice for a 60° triangular grid with elements spaced $d = 1.0$ cm apart was a waveguide diameter of 0.91 cm.

(9) Dielectric cover sheets can move reflection coefficient peaks interior to the grating lobe position unless properly chosen.

2. Computer-aided Optimization Results

The previous observations were based on the results of many computer simulations selected to get physical insight into mutual coupling and impedance matching problems associated with an array of circular waveguide elements. The graphical results of these tests are contained Figs. A- 1 to A- 6 in the Appendix. From these runs it became apparent that the process of matching at broadside was difficult enough, but to choose array parameters to increase usable scan range while maintaining impedance match was next to impossible by human trial-and-error methods. Fortunately remedies exist in the form of computer optimization methods, a good survey of which is given by Bandler [32]. The methods are generally separated into two groups: (1) gradient methods and (2) pattern search methods. Since this problem is too complex to hope gradient information could be determined, a pattern search technique originated by Rosenbrock[32,28] was chosen.

In brief Rosenbrock's method is a coordinate rotation system which for N variable parameters proceeds after each set of N coordinate searches to rotate the coordinates so that the initial increments in the next set of searches are along the vector direction determined by the previous N searches. After each successful move the step size is increased by a factor of three (qualitative choice of Rosenbrock), and a quadratic fit is applied after the first unsuccessful move. The result is an extremely efficient pattern search in that the number of function evaluations from an initial set of "user-chosen" parameter values is kept fairly low. As with all computer optimization techniques this one suffers from the fact that it cannot distinguish a local minimum from an absolute one.

In this application optimizations were made first varying two array parameters and then varying four array parameters. A 60° scan plane for a hexagonal array of elements spaced 1.0 cm. apart was used for investigation. For the unaltered system with guides filled with air and having a radius of 0.44 cm. the reflection coefficient varied from about 0.43 at broadside to a peak of 0.61 at the grating lobe angle ($\theta = 54^\circ$). The cross-polarized reflected mode showed a significant peak of about 0.3 at $\theta = 48^\circ$. The main results of some of the optimizations are summarized as follows:

(1) Varying the dielectric plug (T2 and EPS2) subject to a test function of $|R_1|^2 + |R_2|^2$ at $\theta = 10^\circ$ and 45° the Rosenbrock selections reduced the reflection coefficient peak (R_1) to 0.37 and kept the reflected power in this mode under 4% over the rest of the scan range up to the vicinity of the 54° grating lobe where the peak was located.

(2) Not using matching plugs or dielectric cover sheets but varying guide radius (AX) and dielectric fill (EPS) with the above test function, the Rosenbrock subroutine chose $AX = 0.4555$ and $EPS = 1.495$. With these parameters the reflection coefficient peak was reduced to 0.34 and reflected power was below 5.3% elsewhere.

(3) A really significant improvement in match over the major portion of the scan range was obtained when four parameters were optimized by the Rosenbrock subroutine. In this case the dielectric cover sheet and the guide discs were both used with the resulting choices being $T2 = 0.742$ cm, $EPS2 = 1.19$, $T3 = 0.127$ cm, and $EPS3 = 1.57$. The test function was $|R_1(10^\circ)| + |R_1(54^\circ)|$. The scan for this design showed a slight resonant peak of 11% reflected power at $\theta = 43^\circ$, but reflections were lowered to an almost negligible level of under 0.3% over the scan range away from the peak and were under 0.3% at the grating lobe angle of 54° .

CHAPTER IV

EXPERIMENTAL RESULTS

This chapter summarizes some of the experimental work done which has bearing on phased array matching.

A. Waveguide Simulator

There are many possible approaches to determining the performance of elements in a large phased array. Since a large number of elements is involved, it is desirable to know the performance of various prototype antennas before constructing a whole array of them. If a small array were being designed, measurements could be made on the array after construction and modifications on the individual elements might be achieved with little difficulty. But the number of elements in a large array soon makes this simple approach impractical. There are two basic techniques for modeling a large phased array: a computer analysis, and simulation in a waveguide [18], discussed here.

Recall from the geometry of planar phased arrays that the scan angle is defined as the angle of the beam maximum from broadside and that there are both E and H plane scans. The well known concept of component waves in a rectangular waveguide leads to a method of simulating an infinite planar phased array. Consider the rectangular waveguide shown on the following page, and for simplicity, consider only the dominant TE_{10} mode whose field equations are

$$H_z = A \cos\left(\frac{\pi}{a} x\right) e^{-j\beta z}$$

$$H_x = j \frac{\beta}{K_c} A \sin\left(\frac{\pi x}{a}\right) e^{-j\beta z} \quad (4-1)$$

$$E_y = -jA \frac{K_o}{K_c} Z_o \sin\left(\frac{\pi x}{a}\right) e^{-j\beta z}$$

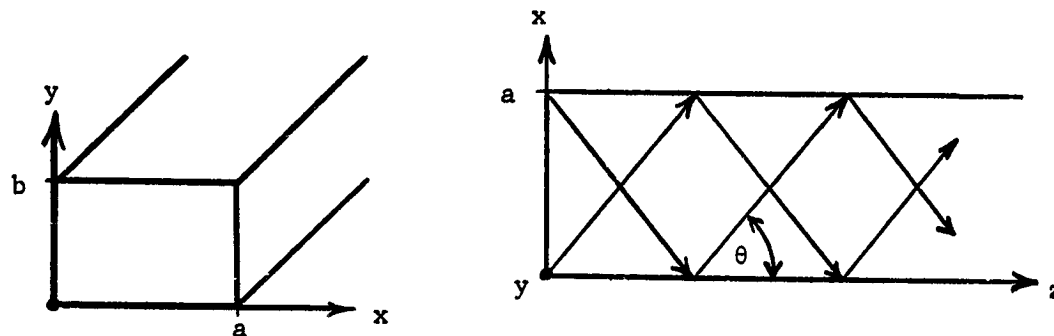


Fig. 4-1. Rectangular Guide with Component Waves.

The expression for H_z may be written as

$$H_z = \frac{A}{2} \left\{ e^{j\left(\frac{\pi x}{a} - \beta z\right)} + e^{-j\left(\frac{\pi x}{a} + \beta z\right)} \right\} \quad (4-2)$$

indicating the two traveling waves shown in Fig. 4-1. Recall the separation equation

$$k_c^2 = k_x^2 + k_y^2 \quad (4-3)$$

For the case of the TE_{10} mode

$$k_c^2 = k_x^2 = \left(\frac{\pi}{a}\right)^2 \quad (4-4)$$

$$k_y = 0.$$

The propagation constant, β , is given by

$$\beta^2 = k_o^2 - k_c^2 \quad (4-5)$$

where $k_o = \omega \sqrt{\mu_o \epsilon_o}$. Thus

$$k_o^2 = \beta^2 + k_c^2 \quad (4-6)$$

Referring to Fig. 4-1,

$$\begin{aligned} k_c &= k_o \sin \theta \\ \beta &= k_o \cos \theta \end{aligned} \quad (4-7)$$

From Eq. (4-7),

$$\sin \theta = \frac{k_c}{k_o} \quad (4-8)$$

The general expression for k_c is $2\pi/\lambda_c$, where λ_c is the cutoff wavelength. Eq. (4-8) now becomes

$$\sin \theta = \frac{\lambda}{\lambda_c} \quad (4-9)$$

This phenomenon in the rectangular waveguide is similar to the operation of a phased array element. The angle θ in Fig. 4-1 may be considered as the "scan angle" from broadside, and various E or H plane scans may be simulated by exciting proper modes in specially built guides. For TE modes, H plane scans are simulated, while E plane scans are achieved by exciting TM modes. By varying the frequency and guide dimensions according to Eq. (4-9), a number of possible scan conditions may be modeled.

The phased array simulation documented in this report was for a square grid of circular waveguides opening onto a conducting ground

plane. The geometry of the simulated array is shown in Fig. 4-2.

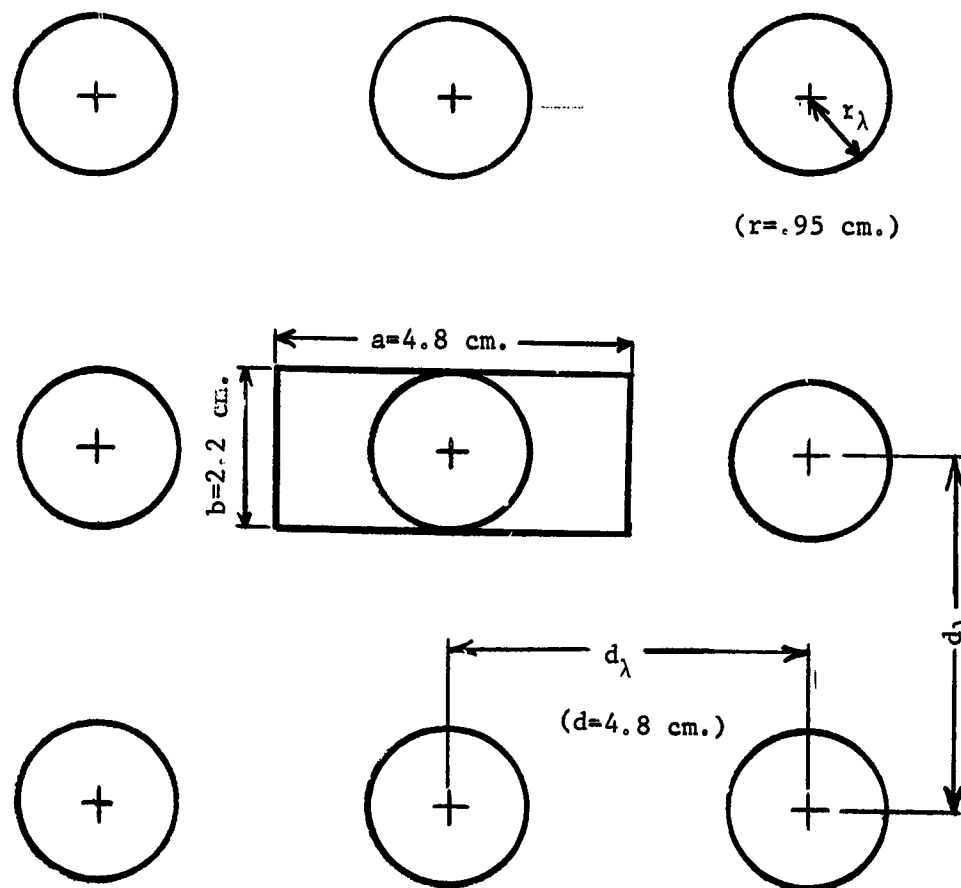


Fig. 4-2. Geometry of Simulated Phased Array.

Notice the waveguide cross section drawn around the central element. By constructing a circular guide to be flush mounted against the rectangular guide and varying the frequency of the field incident on the circular guide, the performance of several different scan

conditions may be studied. Note, however, that varying the frequency changes the relative dimensions of the simulated array. The experimental setup, illustrated in Fig. 4-3, was used to determine the reflection coefficient, Γ , for several different frequencies.

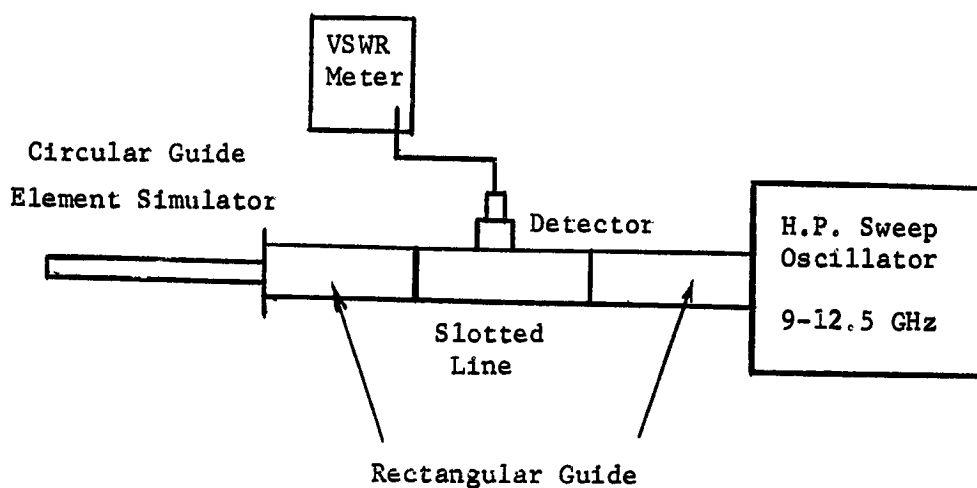


Fig. 4-3. Waveguide Simulator Test Setup.

The range of frequencies used in the experiment were chosen to be above the rectangular guide cutoff but below cutoff for the circular guide. This was done so that a matching scheme at the end of the circular guide was unnecessary.

A sample calculation for a scan condition is shown below.

SAMPLE CALCULATION

For a frequency of 9 GHz

$$\lambda = \frac{c}{f} = 3.33 \text{ cm.}$$

For TE_{10} mode (H-plane scan): $\lambda_c = 2a = 9.6 \text{ cm}$

$$\sin \theta = \frac{\lambda}{\lambda_c} = \frac{3.33}{9.6} = .345$$

Therefore,

$$\theta = 20.3^\circ \text{ (Cardinal Plane Scan)}$$

$$d_\lambda = \frac{d}{\lambda} = \frac{4.8}{3.33} = 1.42$$

$$r_\lambda = \frac{r}{\lambda} = \frac{.95}{3.33} = .286$$

Results obtained from the waveguide simulator were used to check the computer analysis in Chapter III, and agreement was very good. Table I compares the results.

TABLE I
Comparison of Computer and Waveguide Simulator Results
Array of Circular Waveguides

Frequency (GHz)	Scan Angle (H plane)	Reflection Coefficient	
		Waveguide Simulator	Computer Simulation
9.0	20.3°	.980	.962
9.5	19.2°	.930	.936
10.0	18.2°	.890	.900
10.5	17.3°	.865	.880
11.0	16.5°	.900	.870
11.5	15.7°	.861	.858
12.0	15.1°	.855	.850

Despite the good results obtained with the simulator, it has several disadvantages. Since TE modes are most easily generated in rectangular guides, E plane scans are more difficult to achieve than H plane. It is also difficult to get scan planes where grating lobes first appear.

Another problem, mentioned previously, is associated with the transition from the rectangular guide to circular guide. The difficulty arises since the cutoff frequency of the circular guide is usually higher than that of the rectangular guide. If the frequency is high enough above cutoff of the circular guide, unwanted modes in the rectangular guide might be excited. Operating the circular guide above cutoff also requires the design of a matched load section for terminating the circular guide. Exciting the simulator below circular guide cutoff presents still another problem: the reflection coefficients are quite large. In order to obtain meaningful results, the measurements devices must be of sufficiently wide dynamic range.

Perhaps the greatest disadvantage of the waveguide simulator is that a particular array can be modeled at only one scan angle. A thorough investigation of an array would require many simulators and most could not be constructed with standard waveguides. The cost of such an analysis would be prohibitive.

Simulation of a phased array in waveguide can be of significant use, however, especially the way it was employed in this report. Our simulator was easily fabricated, the measurements were simple, and the results were in excellent agreement with our computer analysis. In essence, our waveguide simulator was very useful, because it strongly supported the validity of our computer simulation.

B. Dielectric Cover Sheet Over a Small Array

The impedance of a central element of a 36 element array of crossed slots in a ground plane was measured as a function of scan angle with

and without a dielectric sheet covering the array surface. The array operated at 1.8 GHz with crossed slots for circular polarization positioned as shown in Fig. 4-4. The cover sheet had a dielectric

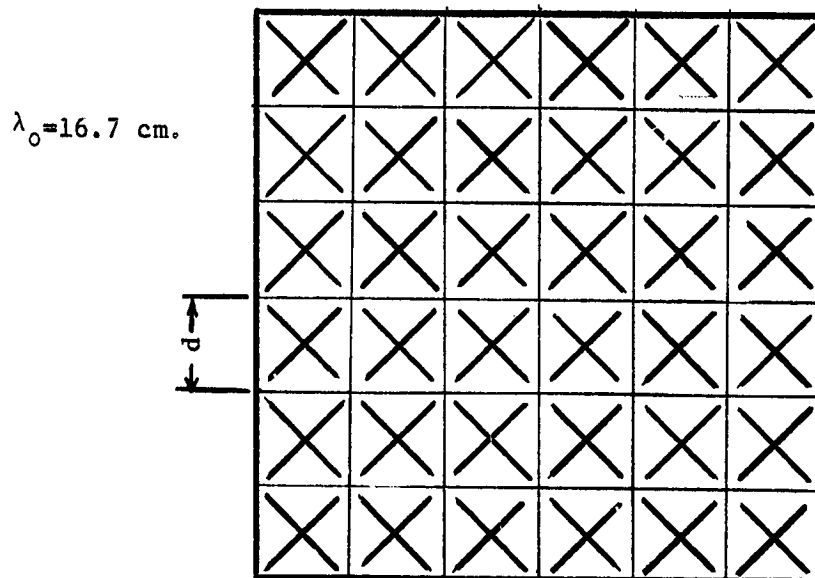


Fig. 4-4. Circularly Polarized Array of Crossed Slots
($f = 1.8 \text{ GHz}$, $d = 7 \text{ cm}$)

constant of 9.0 and a thickness of 0.635 cm. The thickness was an arbitrarily chosen, commercially available value and was not optimally selected for wide angle impedance matching since such a calculation requires "a priori" knowledge of array impedance variations with scan angle. Our experimental results showed that even though introducing the dielectric sheet gave a slightly worse match at broadside than was obtained for the uncovered array, the wide angle scan matches were better for the dielectric covered array.

C. Cavity-Backed Spirals

S-band, cavity-backed spirals were constructed and tested. Impedance versus frequency measurements showed that they had VSWR's under 2 from 2.0 to 3.0 GHz. Several different baluns were built and tested for use with wideband spirals. A detailed discussion of these baluns is found in Technical Report No. 2 [5].

D. Ku-Band Spiral Array

A four-element array of spiral radiators designed for operation with a center frequency of 18.0 GHz was photolithographically produced using gold on an alumina ($\epsilon_r = 9$) substrate.

APPENDIX

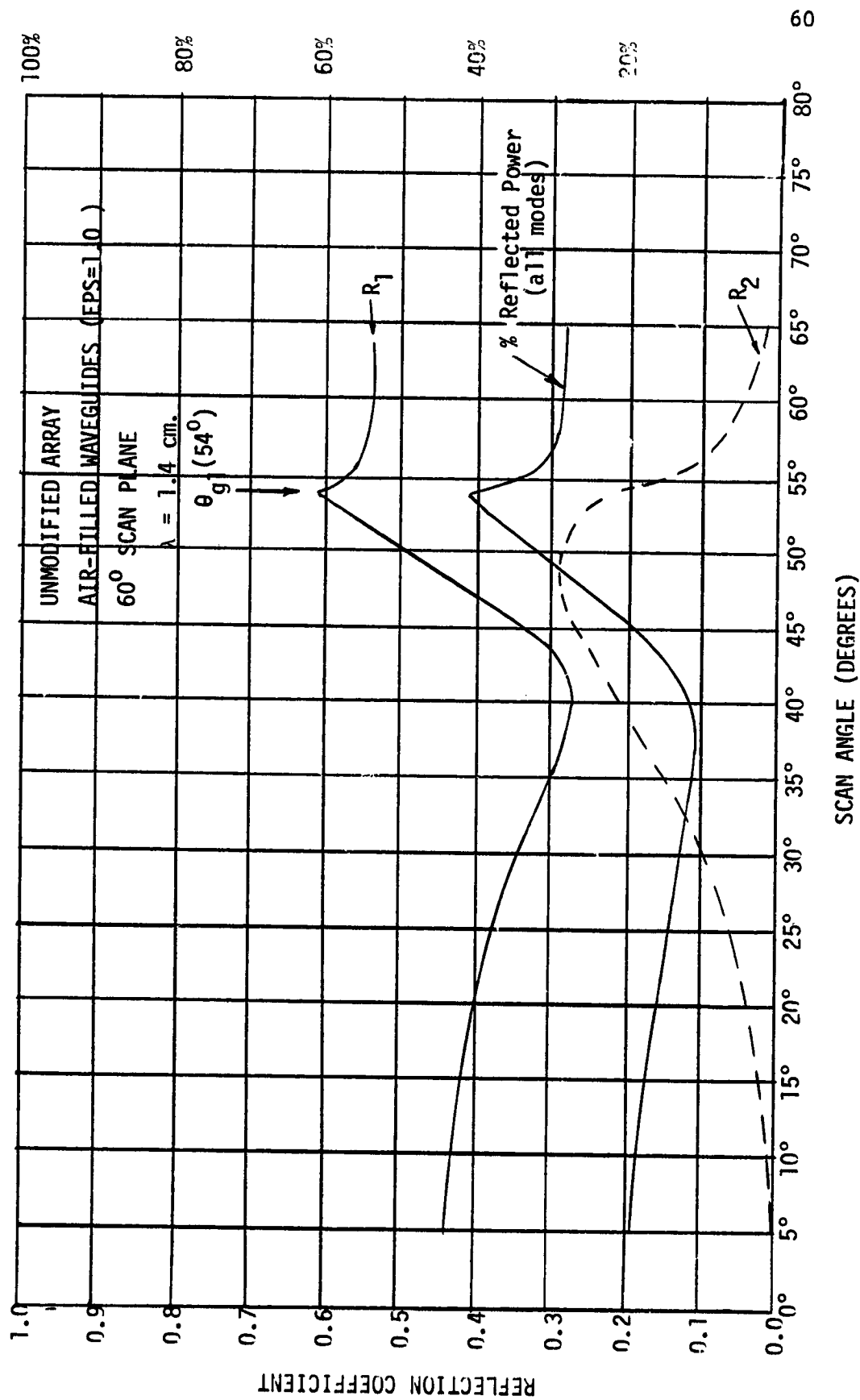


Fig. A-1. Array with Air-Filled Waveguides: 60° Scan Plane, $a=0.44$, $\lambda=1.4$, EPS=1.0, $b=d=1.0$

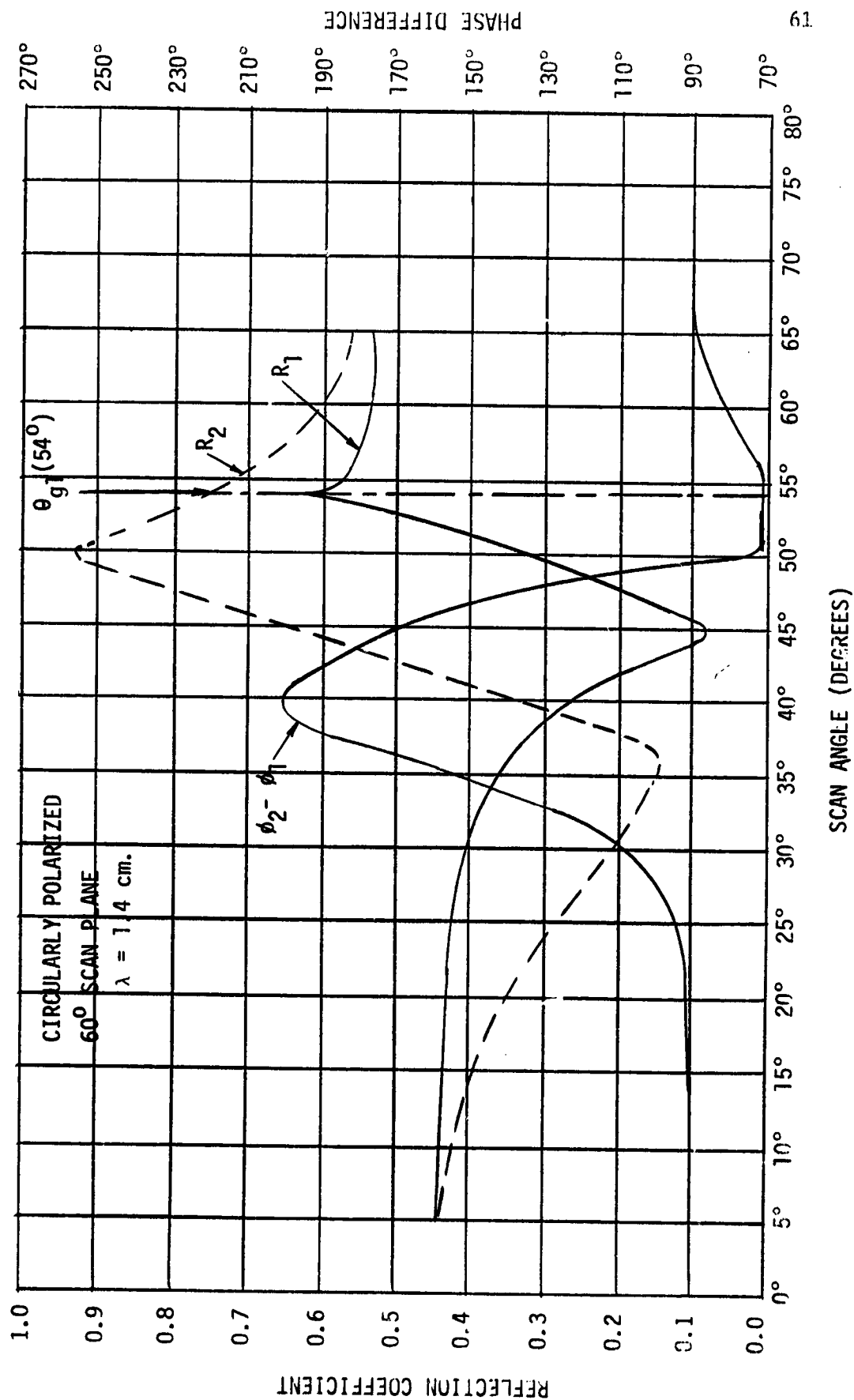


Fig. A-2. Circularly Polarized Array of Circular Waveguide Elements: $a=0.44$ cm, $\lambda=1.4$ cm, $b=d=1.0$ cm, $\text{EPS}=1.0$, $T_2=T_3=0.0$, mode excitation ($I_1=1.0$, $I_2=+j$)

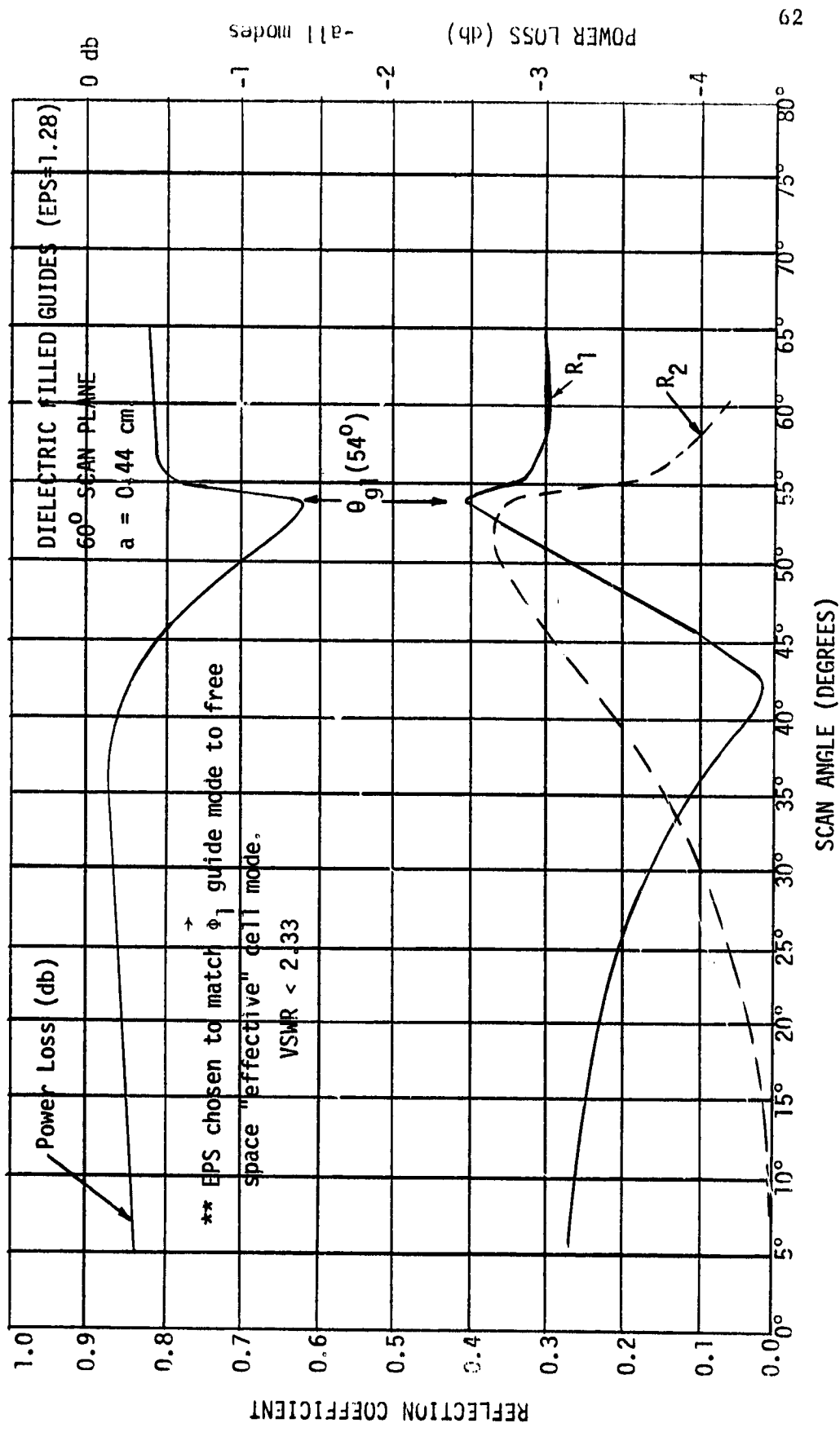


Fig. A-3. Array with Dielectric-Filled Guides: 60° Scan Plane, $a=0.44$, $EPS=1.28$, $\lambda=1.4$, $b=d=1.0$, $T2=T3=0.0$

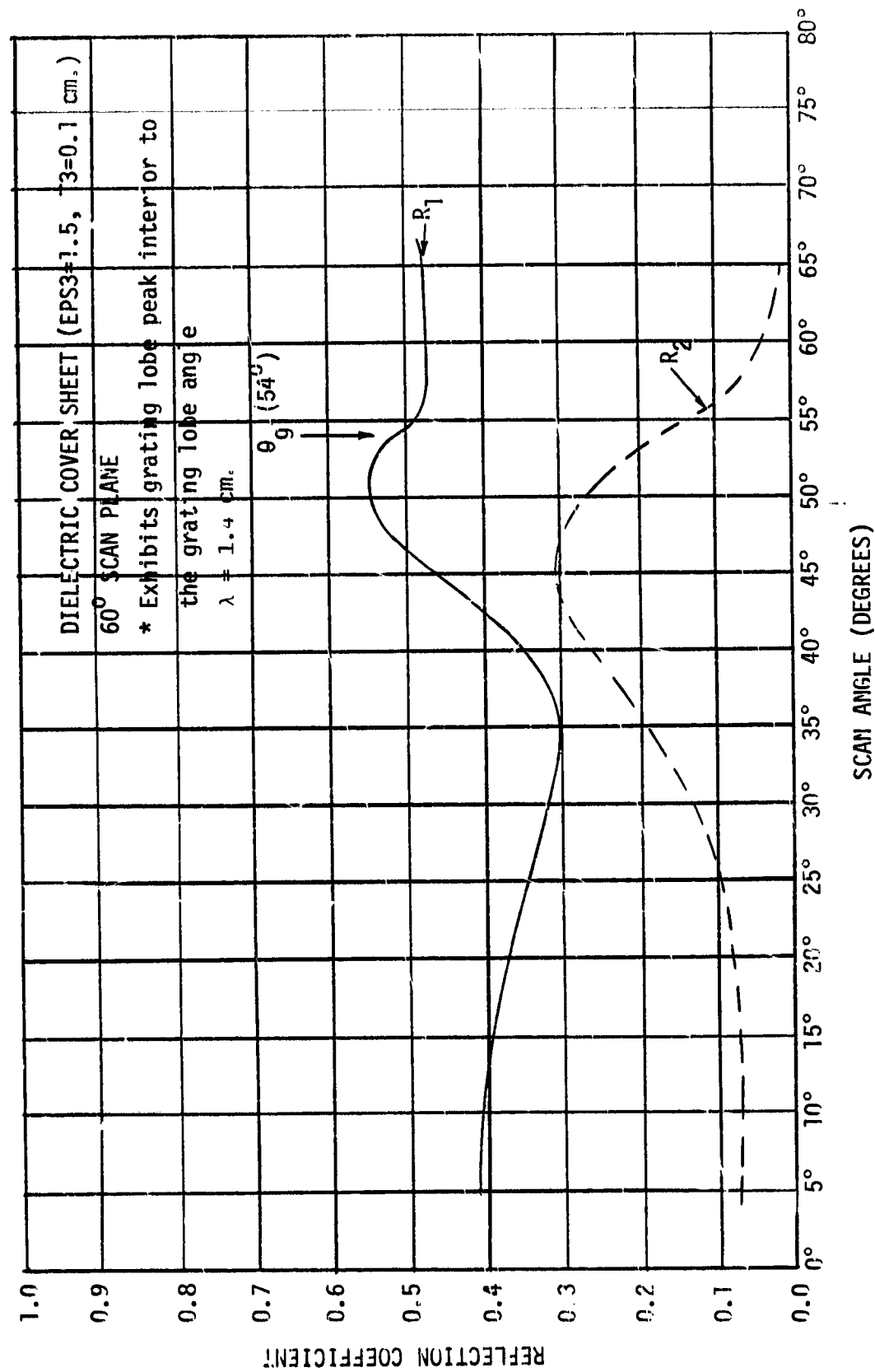


Fig. A-4. Array of Circular Waveguides with Dielectric Cover Sheet: $a=0.44$ cm, $\lambda=1.4$ cm, $b=d=1.0$ cm, $ESP=1.0$, $T3=0.1$, $EPS3=1.5$, $T2=0.0$

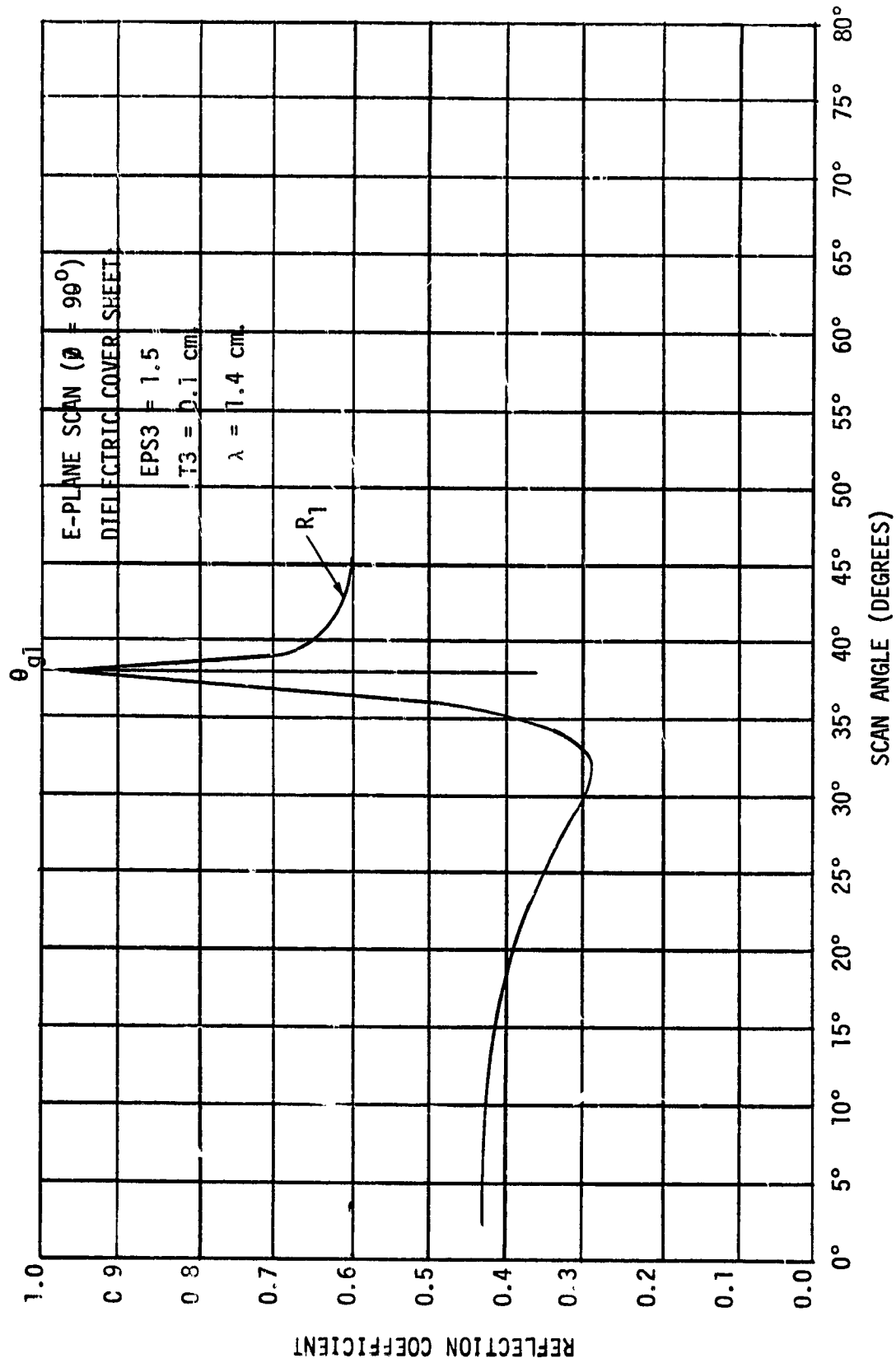


Fig. A-5.E-Plane Scan for Array of Circular Waveguides with Dielectric Cover Sheet:

$a=0.44$ cm, $b=d=1.0$ cm, $\lambda=1.4$, $EPS3=1.5$, $T3=0.1$ cm, $T2=0.0$

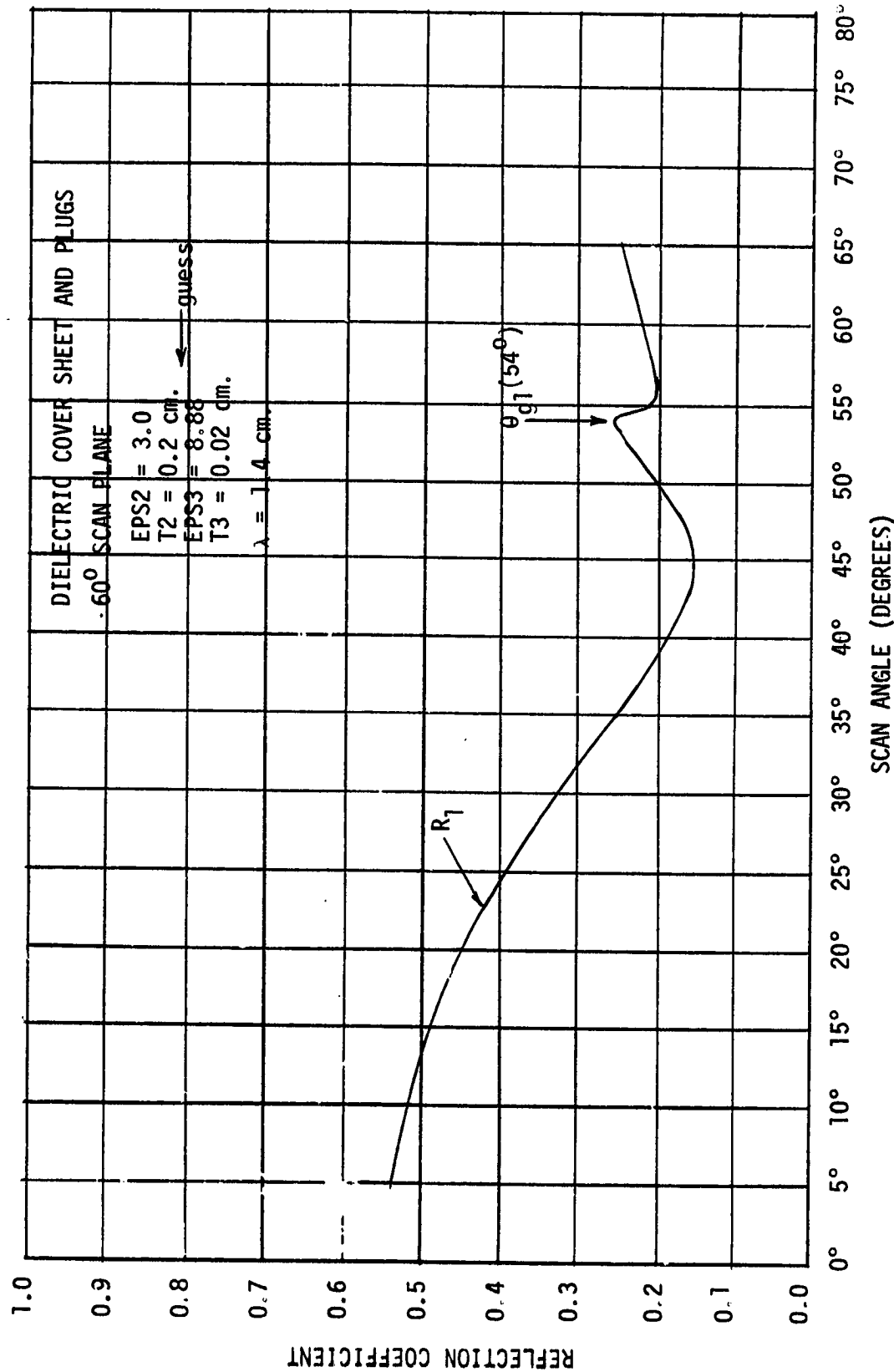


Fig. A-6. Array of Circular Waveguides with Dielectric Cover Sheet and Dielectric Discs
for Matching: $a = -.44$, $b = d = 1.0$, $\lambda = 1.4$, $\text{EPS2} = 3.0$, $T2 = 0.2$, $\text{EPS3} = 8.88$, $T3 = 0.02$

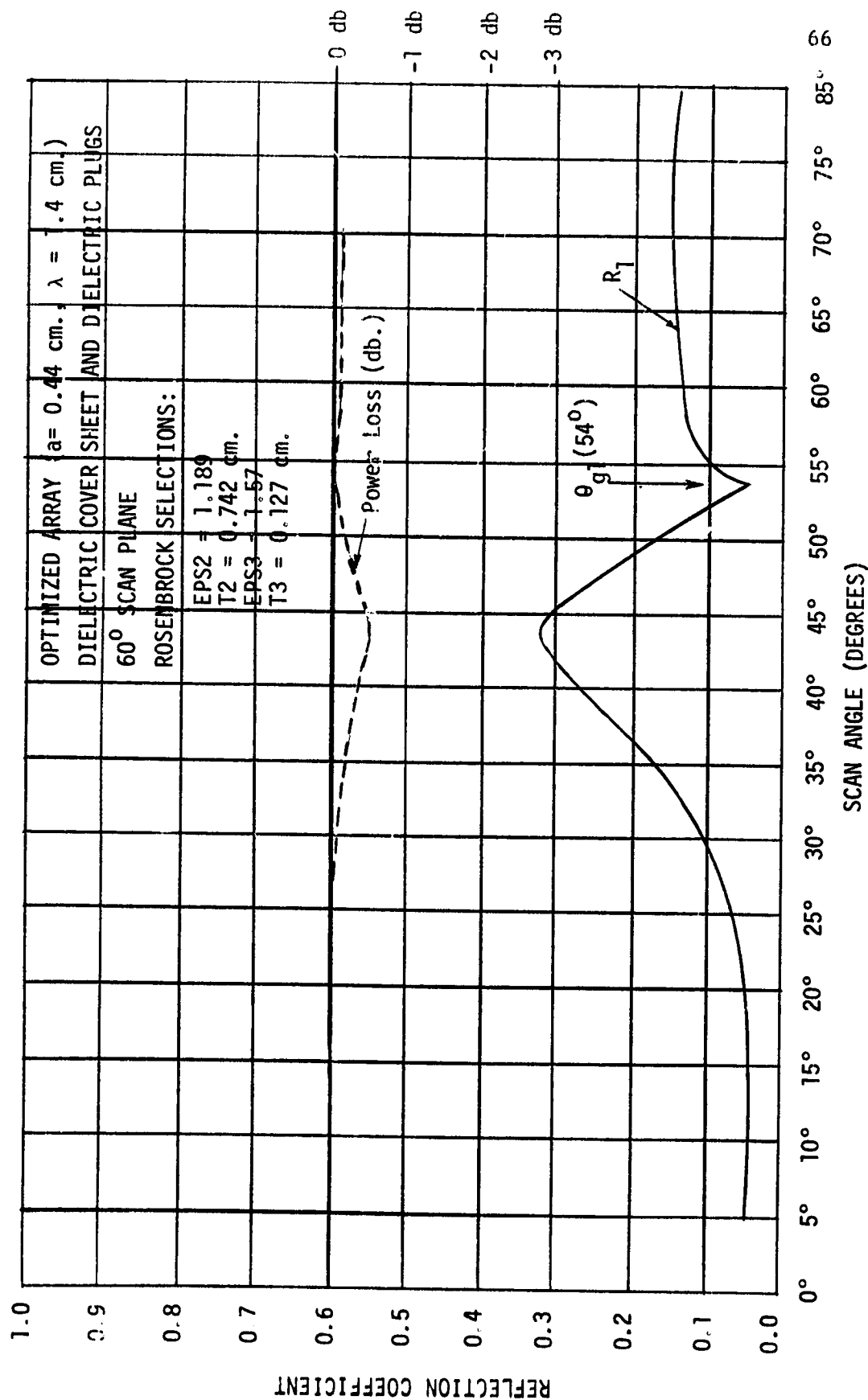


Fig. A-7. Optimized Array with Cover Sheet and Dielectric Plugs for Matching
 $a=0.44$, $b=d=1.0$, $EPS2=1.0$, $EPS2=1.189$, $T2=0.742$, $EPS3=1.57$, $T3=0.127$
 parameters chosen using Rosenbrock subroutine with $TEST=R_1(54)+R_2(10^\circ)$

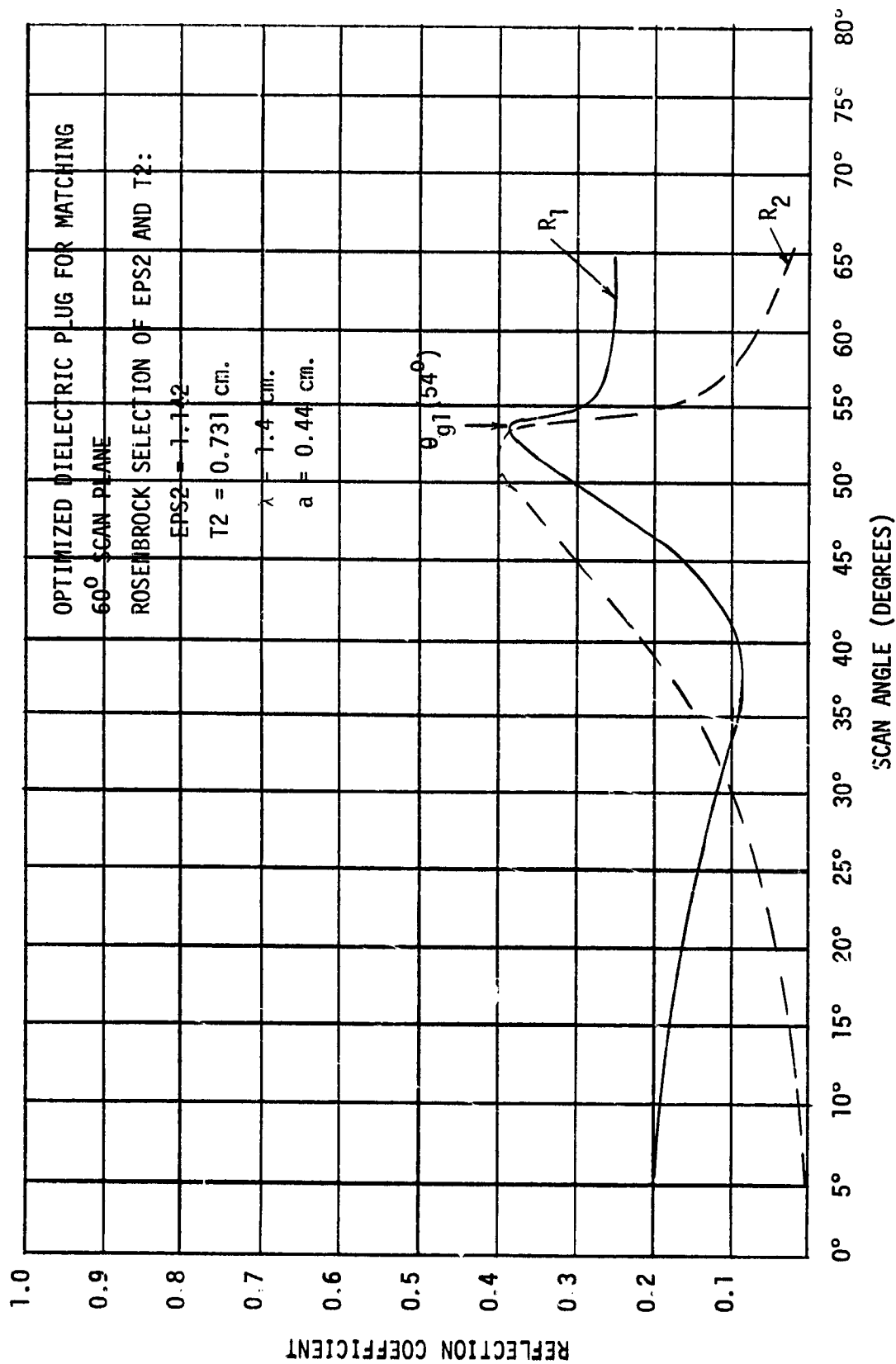


Fig. A-8. REFLECTION COEFFICIENT VS. SCAN ANGLE: infinite array of circular waveguides, equilateral triangular grid, $a=0.44$, $\lambda=1.4$, $b=d=1.0$, $EPS=1.0$, $T2=0.731$, $EPS2=1.142$

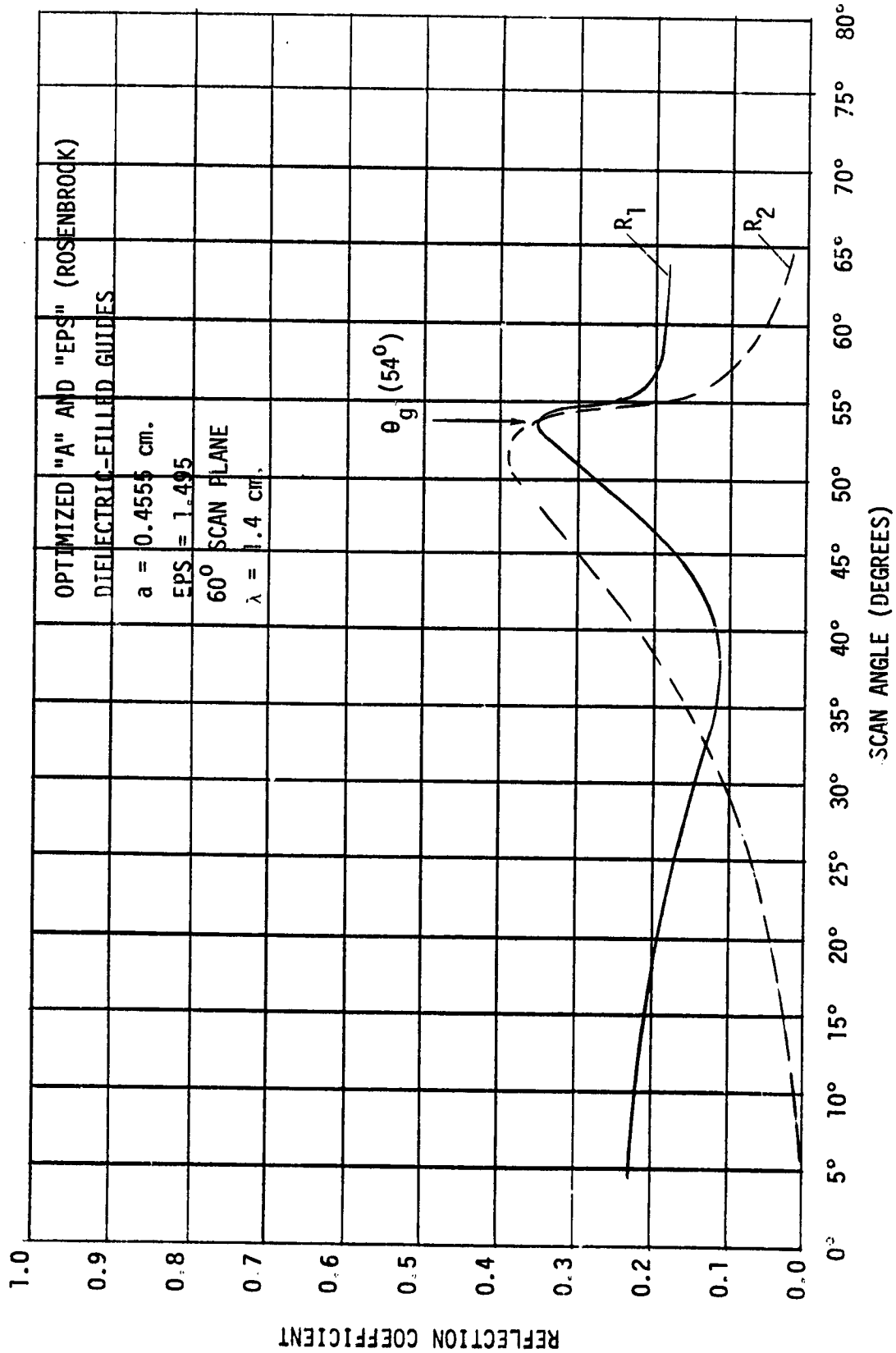


Fig. A-9. Array with Dielectric-Filled Waveguides: optimized (Rosenbrock) radius and dielectric constant, $a=0.4555$, $\text{EPS}=1.495$, $b=d=1.0$, $\lambda=1.4$, $T_2=0.0$, $T_3=0.0$

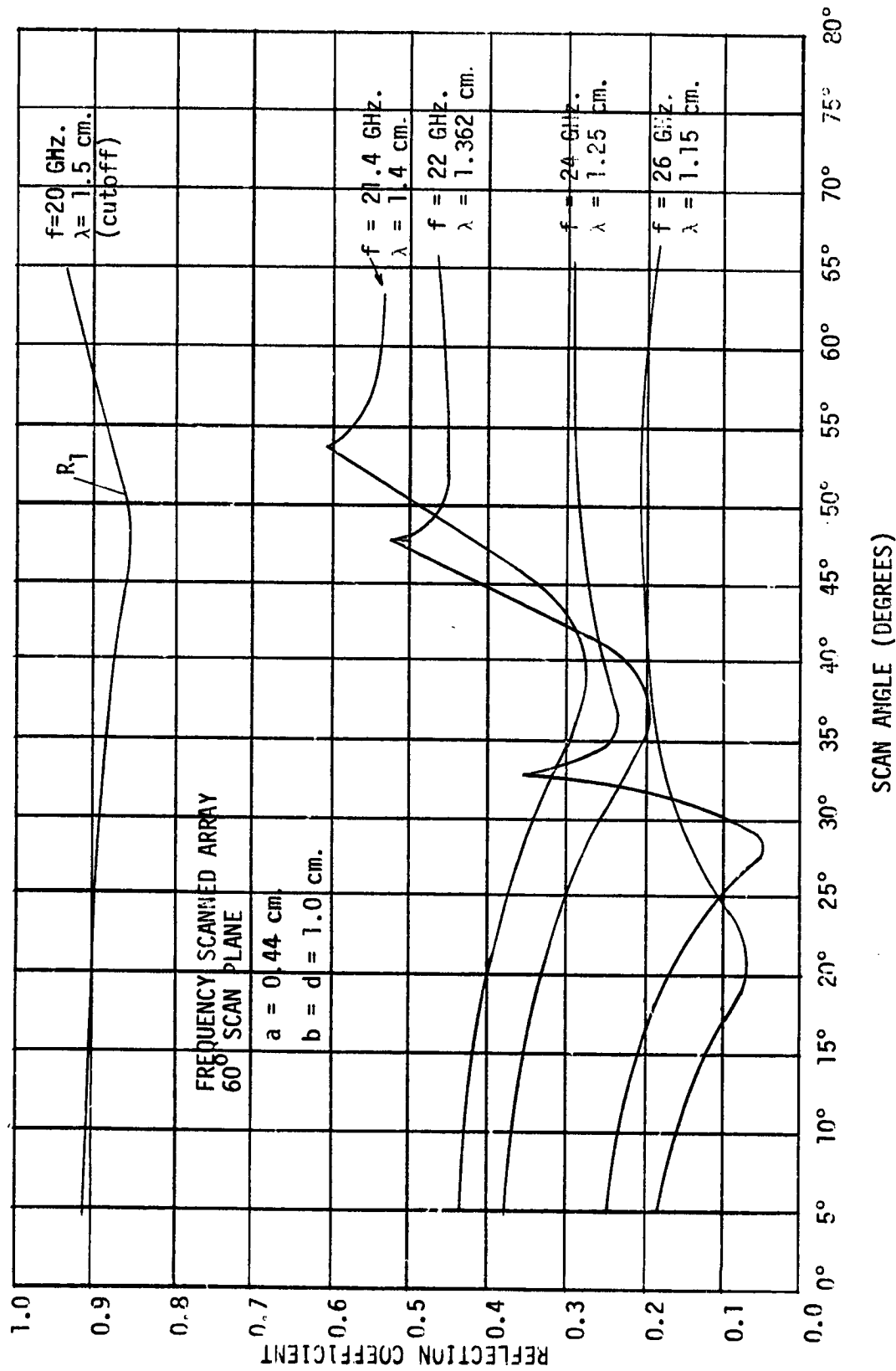


Fig. A-10. Frequency Scanned Array of Air-Filled Guides: $a = 0.44$ cm., $EPS = 1.0$,
 $b = d = 1.0$ cm.

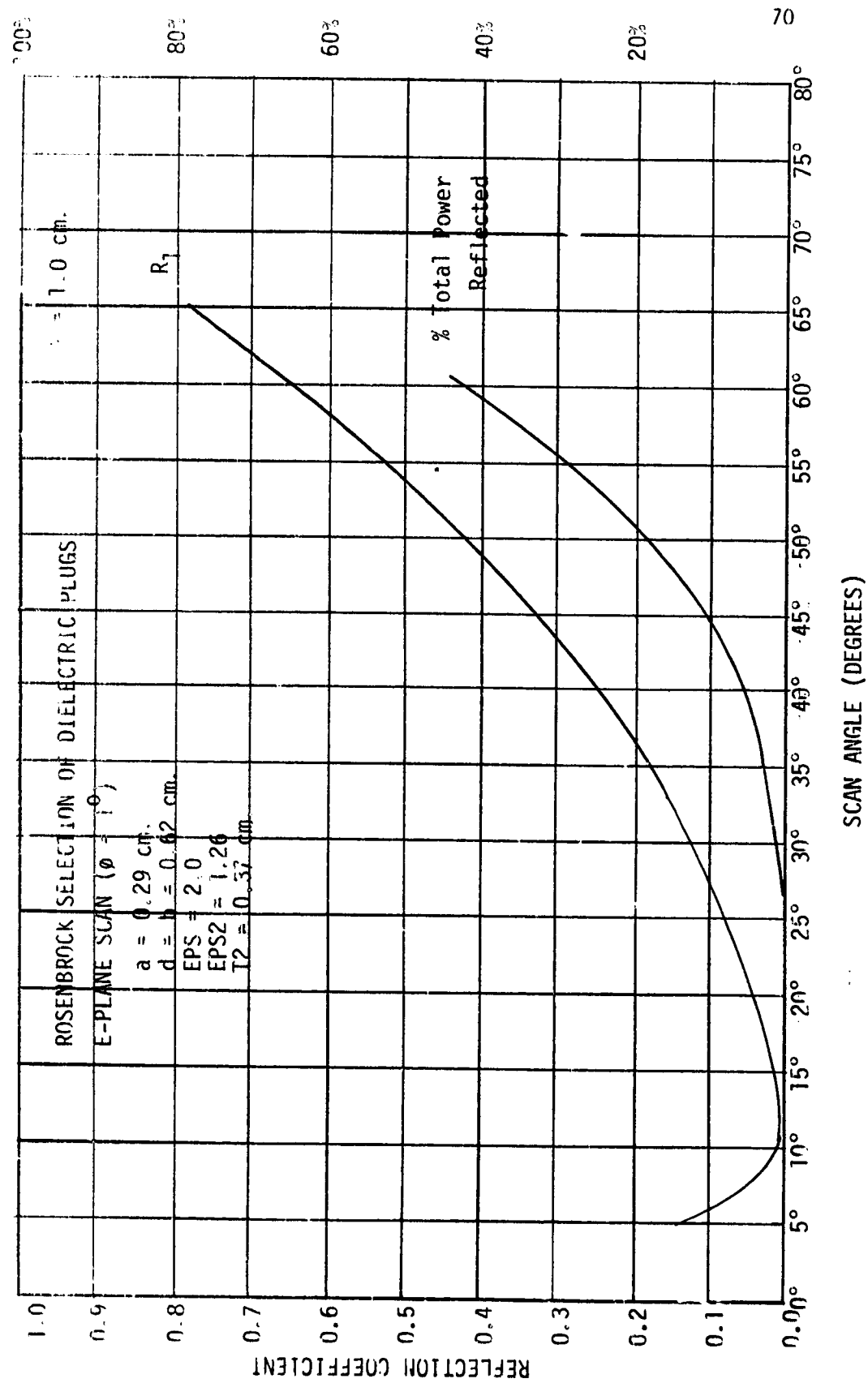


Fig. A-11. Rosenbrock Selection of Dielectric Plugs:

$\lambda = 1.0$ cm., $a = 0.29$ cm., $b = d = 0.62$ cm.

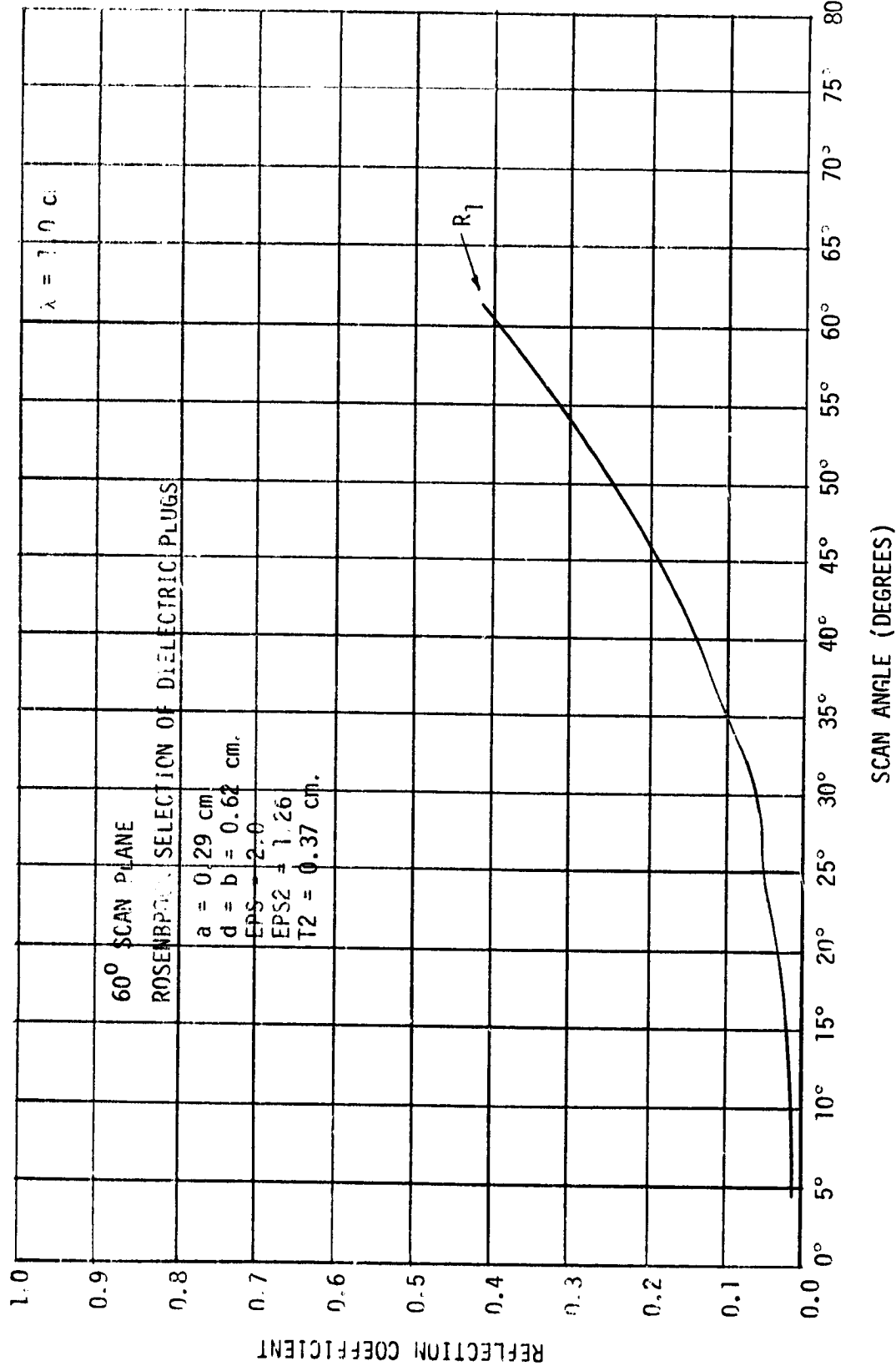


Fig. A-12. 60° Scan Plane: Rosenbrock Selection of Dielectric Plugs
 $a = 0.29 \text{ cm.}, b = d = 0.62 \text{ cm.}, \lambda = 1.0 \text{ cm.}$

REFERENCES

1. J. E. Dudgeon, "Antenna arrays: efficiency and efficiency improvement through compensation," Technical Report No. 1, Contract NAS8-25894, NASA, George C. Marshall Space Flight Center, October 1970, 99 pages.
2. E. G. Magill and H. A. Wheeler, "Wide-angle impedance matching of a planar array antenna by a dielectric sheet," Trans. AP, AP-14, January 1966, pp. 49-53.
3. Hannan, Lerner, and Knittel, "Impedance matching a phased-array antenna over wide scan angles by connecting circuits," Trans. AP, AP-13, January 1965, pp. 28-34.
4. N. Wong, R. Tang, S. W. Lee, and W. R. Jones, "Multimode phased array element for wide scan angle impedance matching," Digest for 1970 Phased-Array Antenna Symposium, June 1970, pp. 66-68.
5. J. Dudgeon and W. D. Daniels, "Microstrip technology and its application to phased array compensation," Technical Report No. 2, NASA Contract NAS8-25894, University of Alabama, January 1972.
6. D. Varon and G. Zysman, BSIJ 46, September 1967, pp. 1561-1586.
7. R. F. Harrington, Field Computations by Moment Methods, MacMillan Press, 1968.
8. P. W. Hannan and M. A. Balfour, "Simulation of a phased array antenna in a waveguide," IEEE Trans. AP, AP-13, May 1965, pp. 342-353.
9. S. W. Lee, "Aperture matching for an infinite circularly polarized array of rectangular waveguides," IEEE Trans. AP, vol. AP-19, May 1971, pp. 332-342.
10. G. H. Knittel, "Wide-angle impedance matching of phased array antennas - A survey of theory and practice," Digest 1970 Phased Array Antenna Symposium, June 1970, pp. 62-67.
11. R. C. Hansen, Microwave Scanning Antennas, Vol. II, Academic Press, 1966.
12. J. L. Allen, "Gain and impedance variation in scanned dipole arrays," IRE T-AP, Vol. AP-10, 1962, pp. 566-573.
13. B. L. Diamond, "Mutual coupling effects in hybrid-fed crossed-dipole arrays," IEEE Int'l Symp. Digest, 1965, pp. 157-163.

14. B. L. Diamond, "Phased array radar studies," July, 1964, MIT, Lincoln Lab Tech. Report TR381.
15. L. Stark, "Radiation impedance of a dipole in infinite phased arrays," Hughes Aircraft Tech. Report No. FL60-230, 1960.
16. L. A. Kurtz, R. S. Elliot, S. Wehn, and W. Flock. "Mutual coupling effects in scanned dipole arrays," IRE-T-AP, Vol. AP-5, 1961, pp. 433-442.
17. J. Bandler and P. Macdonald, "Optimization of microwave network by RAZOR search," IEEE T-MTT, Vol. MTT-17, August, 1969, pp. 552-562.
18. H. A. Wheeler, "A systematic approach to the design of a radiator element for a phased array antenna," Proc. IEEE, Vol. 56, Nov. 1968, pp. 1940-1951.
19. L. Payne and J. Dudgeon, "Simulation of planar spiral antenna elements for phased arrays," Technical Report No. 3, NASA Contract NAS8-25894, University of Alabama, January 1972.
20. R. E. Collin, Foundations of Microwave Engineering, McGraw-Hill, 1966.
21. E. D. Sharp, "A triangular arrangement of planar-array elements that reduces the number needed," IEEE T-AP, Vol. AP-9, March 1961, pp. 126-129.
22. N. Amitay and V. Galindo, "The analysis of circular waveguide arrays," BSTJ, Nov. 1968, pp. 1903-1932.
23. G. V. Gorgiotti and Q. Balzano, "Analysis of periodic phased arrays of circular apertures," T-AP, Vol. AP-17, March 1969, pp. 224-226.
24. S. W. Lee, W. R. Jones and J. J. Campbell, "On the convergence of numerical solutions in iris-type discontinuities," Hughes Aircraft Tech Report FR 70-14-594, August 1970, Fullerton, California.
25. R. Mittra and S. W. Lee, notes from text on numerical solutions in waveguide problems, to be published.
26. R. F. Harrington, Time Harmonic Electromagnetic Fields, McGraw-Hill, 1961, pp. 129-132.
27. J. Dudgeon, "Antenna arrays: efficiency and efficiency improvement through compensation," Tech. Report No. 1 on NAS8-25894, October 1970.
28. T. Trick and J. Vlach, "Computer-aided design of broad-band amplifiers with complex loads," IEEE T-MTT, September 1970, pp. 541-547.
29. T. C. Cheston and J. Frank, ed. M. I. Skolnik, Radar Handbook, Chapter 11, McGraw-Hill, 1970.

30. J. Frank, "Bandwidth Criteria for Phased Array Antennas," Digest for 1970 Phased-Array Antenna Symposium, Polytechnic Inst. of Brooklyn, June 1970.
31. A. Lavi and T. Vogel, Recent Advances in Optimization Techniques, John Wiley, pp. 23-44.
32. J. W. Bandler, "Optimization methods for computer-aided design," IEEE Transactions on Microwave Theory and Techniques, August 1969, pp. 533-551.
33. R. Bawer and J. Wolfe, "The spiral antenna," 1960 IRE Convention Record, part 2, pp. 84-95.
34. J. A. M. Lyon et al., "Derivation of aerospace antenna coupling-factor interference prediction techniques," AFAL-TR-66-57, April 1966, pp. 49-67.
35. R. F. Harrington and J. Mautz, "Computations for linear wire antennas and scatterers," Tech. Report No. RADC-TR-66-351, vol. II, Rome Air Development Center, DDC No. AD 639745, August, 1966.
36. C. P. Wu and V. Galindo, "Properties of a phased array of rectangular waveguides with thin walls," IEEE Trans. Antennas and Propagation, vol. AP-14, March, 1966, pp. 163-170.
37. V. Galindo and C. P. Wu, "Dielectric loaded and covered rectangular waveguide phased arrays," BSTJ, vol. 47, 1968, pp. 93-116.
38. S. W. Lee and W. R. Jones, "On the suppression of radiation nulls and broadside impedance matching of rectangular waveguide phased arrays," IEEE T-AP, vol. AP-19, January, 1971, pp. 41-51.
39. G. Farrell Jr. and D. H. Kuhn, "Mutual coupling in an infinite array of rectangular waveguide horns," IEEE T-AP, vol. AP-16, July, 1968, pp. 405-414.
40. E. Graf and J. Johnson, "Antenna elements that enable a phased array to be scanned over a hemispherical sector," Auburn Tech. Report 4 on NAS8-205707, June, 1967.